JIET

Journal Of Investigation On Engineering & Technology

VOLUME/ CİLT: 6 (2023)

ISSUE: 1

ISSN: 2687-3052

KTÜ 1955 KARADENİZ TEKNİK ÜNİVERSİTESİ

Journal of Investigation on Engineering & Technology

http://dergipark.gov.tr/jiet

INDEXING:
İndeksler

Product Information
Ürün Bilgisi

Volume *Cilt* **6** **Issue** *Sayı* **1** **June/2022** *Haziran/2022*

Publisher *Yayıncı*	Karadeniz Technical University, Faculty of Technology *Karadeniz Teknik Üniversitesi Of Teknoloji Fakültesi*
Web Page *Web Sayfası*	http://dergipark.gov.tr/jiet
Date of Publication *Basım Tarihi*	June /2023 *Haziran/2023*
Language *Yayın Dili*	English/Turkish *İngilizce/Türkçe*
Frequency *Yayın Aralığı*	Published twice in a year *Yılda iki kez yayınlanır*
Type of Publication *Yayın Türü*	Periodical *Süreli yayın*
ISSN Number *ISSN Numarası*	2687-3052

Yazışma Adresi
Karadeniz Teknik Üniversitesi
Teknoloji Fakültesi
Çamlı M. Hacı Mehmet Baheddin Ulusoy
Cad. No:144 61830 Of / TRABZON
Telefon: +90 462 377 83 01
E-posta: jiet@ktu.edu.tr

Correspondence Address
Karadeniz Technical University
Faculty of Technology
Çamlı M. Hacı Mehmet Baheddin Ulusoy
St. No:144 61830 Of / TRABZON
Phone: +90 462 377 83 01
E-mail: jiet@ktu.edu.tr

Makale gönderimi dergipark üzerinden yapılmaktadır. Tüm yayınlanan makalelere http://dergipark.gov.tr/jiet adresinden ulaşılabilir.

Paper submission is done via dergipark. All published papers are available at http://dergipark.gov.tr/jiet .

CONTENTS

İçindekiler

Journal of Investigations on Engineering & Technology
Volume 6, Issue 1, 1-12, 2023

ISSN: 2687-3052

Araştırma Makalesi

Tüketicilerde Kaçak Elektrik Kullanımının Akıllı Sayaç Verisi Üzerinden Gradyan Artırmalı Karar Ağacı Tabanlı Makine Öğrenmesi Yöntemleriyle Tespiti

Yasin Kara[1], Ayşe Aksu[1]

(Alınış / Received: 07.04.2023, Kabul / Accepted: 23.05.2023, Online Yayınlanma / Published Online: 26.07.2023)

Anahtar Kelimeler
Akıllı sayaçlar
Güç sistemleri
Kaçak elektrik
Karar ağaçları
Makine öğrenmesi
Teknik olmayan kayıplar

Öz: Elektrik enerjisinin iletimi ve dağıtımında meydana gelen teknik olmayan kayıplardan başlıcası olan kaçak elektrik kullanımı, tüm dünyada karşılaşılan ciddi bir sorundur. Kaçak elektrik kullanımı, toplumun tüm kesimlerine ekonomik ve sosyal zararlar verdiği gibi elektrik arz güvenliğini de tehdit etmektedir. Son zamanlarda dünya genelinde kullanımı giderek artan akıllı sayaç teknolojisi, kaçak elektrik kullanımının veri güdümlü tespiti için yeni olanaklar sağlamaktadır. Bu çalışmada, tüketicilerde gerçekleşen kaçak elektrik kullanımının akıllı sayaç verileri üzerinden tespiti amacıyla, gradyan artırmalı karar ağacı tabanlı üç makine öğrenmesi modeli ele alınmıştır. Bu anlamda, LightGBM, XGBoost ve CatBoost modelleri kullanılmış ve modeller, akıllı sayaçlardan okunan tarihsel günlük elektrik tüketim verileri üzerinden ilgili tüketicinin elektrik kullanımını "yasal kullanım" veya "kaçak kullanım" olarak sınıflandırması amacıyla eğitilmiştir. Çalışmada, Çin Devlet Elektrik Şirketi'nin yayımladığı, eksik ve dengesiz veriler içeren gerçek akıllı sayaç veri kümesi kullanılmıştır. Başarım denetleme çalışmaları, CatBoost modelinin doğruluk ve AUC ölçevlerinde sırasıyla %78,10 ve %74,17, LightGBM modelinin ise duyarlılık ölçevinde %72,48 değeri ile diğer modellere kıyasla daha yüksek başarımlı oluğunu göstermiştir.

Detection of Electricity Theft in Consumers through Gradient Boosting Decision Tree-based Machine Learning Methods using Smart Meter Data

Keywords
Smart meters
Power systems
Electricity theft
Decision trees
Machine learning
Non-technical losses

Abstract: Electricity theft, which is one of the major non-technical losses in the transmission and distribution of electricity, is a serious problem encountered worldwide. Electricity theft causes economic and social losses to all segments of society and also threatens the security of electricity supply. Recently, increasing use of smart meter technology worldwide provides new opportunities for data-driven detection of electricity theft. In this work, three machine learning models based on gradient boosting decision trees, LightGBM, XGBoost, and CatBoost, are adopted for the detection of electricity theft in consumers through smart meter data. The models are trained to classify the consumer's electricity usage as "legal usage" or "theft

[1] Çözümevi Yönetim Danışmanlığı ve Bilgisayar Yazılım Ticaret A.Ş, Orta Mah. Ordu Sok. İzpark Plaza No: 23/A İç Kapı No: 13, 34880 Kartal İstanbul/Türkiye

Sorumlu yazar ve e-posta adresi: Ayşe Aksu / rnd@cozumevi.com

usage" using historical daily electricity consumption data obtained from smart meters. In the study, a real smart meter dataset published by the State Grid Corporation of China, which contains missing and unbalanced data, is used. The performance evaluation studies reveal that the CatBoost model achieved higher accuracy and AUC of 78.10% and 74.17%, respectively, while the LightGBM model achieved higher recall value of 72.48%, compared to the other models.

1. Giriş

Elektrik enerjisinin üretiminden başlayarak son kullanıcıya ulaştırılmasına kadar gerçekleşen tüm süreçlerde meydana gelen enerji kayıpları, tamamen bertaraf edilmesi mümkün olmayan bir olgudur. Elektrik enerjisi kayıpları, teknik ve teknik olmayan kayıplar olarak iki sınıfta incelenebilir. Teknik kayıplar temel olarak, iletim hattı, kablo, transformatör ve sayaç gibi elektriksel elemanların direnci nedeniyle açığa çıkan ısı enerjisinden ileri gelmektedir. Teknik kayıplar, verimli eleman seçimi ve uygun planlama ile en aza indirilebilse de tamamen sıfırlanması mümkün olmayan fiziksel bir fenomendir.

Teknik olmayan kayıplar ise, elektrik hırsızlığı (kaçak elektrik kullanımı), sayaçların hatalı çalışması ya da okunması veya eksik faturalama gibi durumların sonucudur [1]. Ülkemizde yürürlükte olan 6446 numaralı Elektrik Piyasası Kanunu, teknik ve teknik olmayan kayıpları,

> *"Dağıtım sistemine giren enerji ile dağıtım sisteminde tüketicilere tahakkuk ettirilen enerji miktarı arasındaki farkı oluşturan ve maliyeti etkileyen; teknik kayıp ve/veya kaçak kullanım gibi sebeplerden kaynaklanan ve teknik bir sebebe dayanmayan kayıp"*

olarak tanımlamıştır [2]. Teknik olmayan kayıpların, teknik kayıpların aksine, sıfıra indirilmesi kuramsal olarak mümkündür [3].

Teknik olmayan kayıplardan başlıcası olan kaçak elektrik kullanımı, tüm dünyada, özellikle de gelişmekte olan ülkelerde karşılaşılan ciddi bir sorundur. Yapılan araştırmalar, dünya genelinde kaçak elektrik kullanımının yılda yaklaşık 90 milyar $ maddi zarar meydana getirdiğini ortaya koymaktadır [4]. TEDAŞ verilerine göre Türkiye genelinde 2019 yılında elektrik enerjisi kayıpları oranı %12,7 olarak gerçekleşmiştir [5]**.** Teknik olmayan kayıpların bu yüzde içindeki ağırlığı belirtilmemiş olsa da kaçak elektrik kullanımının özellikle kimi illerde %60 mertebelerine ulaştığı bilinmektedir [6].

Kaçak elektrik kullanımı bir yandan toplam elektrik üretim yükünü, bir yandan da meşru (yasal) elektrik tüketicilerinin enerji giderlerini (kayıp/kaçak bedeli benzeri kalemler üzerinden) arttırdığından, toplumun hemen her kesimine ekonomik zararlar vermektedir [7]. Bunların ötesinde, kaçak kullanım için elektrik tesisatı üzerinde yapılan sayaç baypası ve kaçak hat çekilmesi gibi yetkisiz müdahaleler, elektrik tüketicileri için hayati tehlike oluşturmaktadır [8,9]. Ayrıca ülkemizde yapılan bir çalışmada, kaçak elektrik kullanımının enterkonnekte sistem genelinde gerilim çökmesi gibi enerji kalitesi problemlerine yol açabildiği gösterilmiştir [10]. Bu bilgilerden hareketle, kaçak elektrik kullanımının önlenmesinin, ekonomik ve toplumsal yitimlerin önlenmesi açısından büyük önem arz ettiği görülmektedir. Kaçak kullanımların en aza indirilebilmesi için atılacak adımların başında, süregelen bir kaçak elektrik kullanımının tespit edilmesi gelmektedir.

Dünyada kullanımı giderek artan akıllı sayaç (smart meter) teknolojisi, tüketici-şebeke işletmecisi arası iki yönlü haberleşme ile yüksek doğruluk ve sıklıkta veri aktarımına imkân sağlamaktadır [11,12]. Böylelikle, şebeke işletmecileri tarafından temin edilen tüketim verileri, veri güdümlü yöntemlerle işlenerek, tüketici tarafında var olan çeşitli anomalilerin tespiti için kullanılabilmektedir [13]. Bu anlamda, son yıllarda başarımları giderek artan ve hemen her alanda yaygın kullanım alanı bulunan makine öğrenmesi yaklaşımları, tüketici tarafında meydana gelen kaçak elektrik kullanımlarının akıllı sayaç verisine dayalı olarak tespiti için uygun bir aday haline gelmiştir. Makine öğrenmesi modelleri, akıllı sayaçlardan elde edilen tüketim verileri ile eğitilerek, kaçak ve yasal kullanım örüntülerini öğrenebilir [14]. Eğitilen makine öğrenmesi modeli, eğitim kümesinde bulunmayan tüketim verileri üzerinde tahmin yaparak kaçak elektrik kullanımını tespit amacıyla kullanılabilir.

Kaçak elektrik kullanımının makine öğrenmesi modelleri ile tespiti problemi, özellikle son yıllarda literatürde geniş çaplı olarak irdelenmiştir. Bu anlamda, gözetimli (supervised), yarı-gözetimli (semi-supervised) ve gözetimsiz (unsupervised) öğrenme problemleri kurgulanmış ve çeşitli makine öğrenmesi modelleri ele alınmıştır [15].

Kullanılan gözetimli öğrenme modelleri arasında, yapay sinir ağı tabanlı uzun kısa-dönem hafızalı sinir ağları [15], çok katmanlı derin sinir ağları [16], evrişimli sinir ağları [17] ve yinelemeli sinir ağları [18] bulunmaktadır. Öte

yandan, karar ağaçları [19], rastsal ormanlar [20] ve destek vektör makineleri [21] gibi modeller de ele alınmıştır. Yarı gözetimli problemler için RDAE-AG-TripleGAN [22] ve derin öğrenme [23] tabanlı hibrid modeller önerilmiştir. Kurgulanan gözetimsiz öğrenme problemlerinin çözümünde ise hiyerarşik kümeleme [24] ve k-ortalamalar [25] gibi kümeleme yöntemleri kullanılmıştır.

Bu çalışmada, tüketicilerde gerçekleşen kaçak elektrik kullanımlarının akıllı sayaç verileri üzerinden tespiti amacıyla, gradyan artırmalı karar ağacı (gradient boosting decision trees) tabanlı üç ayrı makine öğrenmesi modeli önerilmiştir. Bu anlamda, LightGBM, XGBoost ve CatBoost modelleri ele alınmıştır. Modeller, akıllı sayaçlardan okunan tarihsel günlük elektrik tüketim verileri üzerinden, ilgili tüketicinin elektrik kullanımını "yasal kullanım" veya "kaçak kullanım" olarak sınıflandırması amacıyla eğitilmiştir. Çalışmada, Çin Devlet Elektrik Şirketi'nin yayımladığı gerçek akıllı sayaç verileri kullanılmıştır.

Makalenin geri kalan kısımları şu şekilde düzenlenmiştir: Kısım 2'de çalışmada kullanılan veri kümesi tanıtılmış, ele alınan makine öğrenmesi modelleri ile bu modellerin eğitimi, üstparametre optimizasyonu, sınanması ve başarım değerlendirmesi süreçleri detaylandırılmıştır. Kısım 3'te üstparametre optimizasyonu ve sınama kümesi üzerindeki bulgular paylaşılmıştır. Son olarak Kısım 4'te tartışma ve sonuçlara yer verilmiştir.

2. Materyal ve Metot

2.1. Veri kümesi

Çalışmaya konu olan kaçak elektrik kullanımının akıllı sayaç verisi üzerinden tespiti problemi, bir sınıflandırma problemi olarak kurgulanmıştır. Bir gözetimli öğrenme problemi olan sınıflandırma problemlerinde, makine öğrenmesi modelinin eğitimi için etiketlenmiş bir veri kümesine ihtiyaç vardır. Bu amaçla, [26]'da sunulan veri kümesinden faydalanılmıştır. Veri kümesi, Çin Devlet Elektrik Şirketi'nin [27] yayımladığı gerçek akıllı sayaç verilerini içermektedir. Veri kümesine, ilgili GitHub çevrimiçi deposundan [28] erişilebilmektedir.

Bu veri kümesinde, 42.374 elektrik tüketicisinden 2014 – 2016 yılları arasında 1.034 gün boyunca alınan günlük elektrik enerjisi tüketimi verileri yer almaktadır. Dolayısıyla her bir tüketici bir örnek, her bir günlük tüketim verisi ise bir öznitelik olarak alınmıştır. Veri kümesinde ayrıca, her bir tüketiciye ilişkin "yasal kullanım" (sınıf 0) ve "kaçak kullanım" (sınıf 1) etiketi yer almaktadır. Veri kümesine ilişkin çeşitli istatistikler, Tablo 1'de sunulmuştur. Yasal ve kaçak kullanımlara ilişkin 100'er adet veri örneği, sırasıyla Şekil 1 ve 2'de gösterilmiştir.

Tablo 1. Kullanılan veri kümesine ilişkin istatistikler

Örnek sayısı	Öznitelik Sayısı	Sınıf sayısı (etiketler)	Eksik veri oranı	Kaçak/yasal kullanım örnek oranı
42.374	1.034	2 (kaçak/yasal)	1/3,90	1/10,72

Tablo 1'de görüldüğü üzere veri kümesinde pek çok eksik veri (missing data) bulunmaktadır, yaklaşık her dört veri hücresinden biri eksiktir. Ayrıca, bekleneceği üzere, kaçak kullanıma ilişkin örnekler, yasal kullanıma ilişkin örneklerden çok daha azdır. Bu durum, veri dengesizliği (imbalanced data) durumunu doğurmaktadır. Eksik veri ve veri dengesizliği koşullarında makine öğrenmesi modellerinin eğitiminin güçleştiği ve başarımlarının düştüğü bilinmektedir [29,30]. Dahası, kimi makine öğrenmesi modellerinin (örneğin lojistik regresyon, yapay sinir ağları, destek vektör makineleri) eğitimi, eksik verinin bulunduğu veri kümeleri ile gerçekleştirilememekte ve eksik veri doldurma (imputation) yöntemlerine ihtiyaç duyulmaktadır.

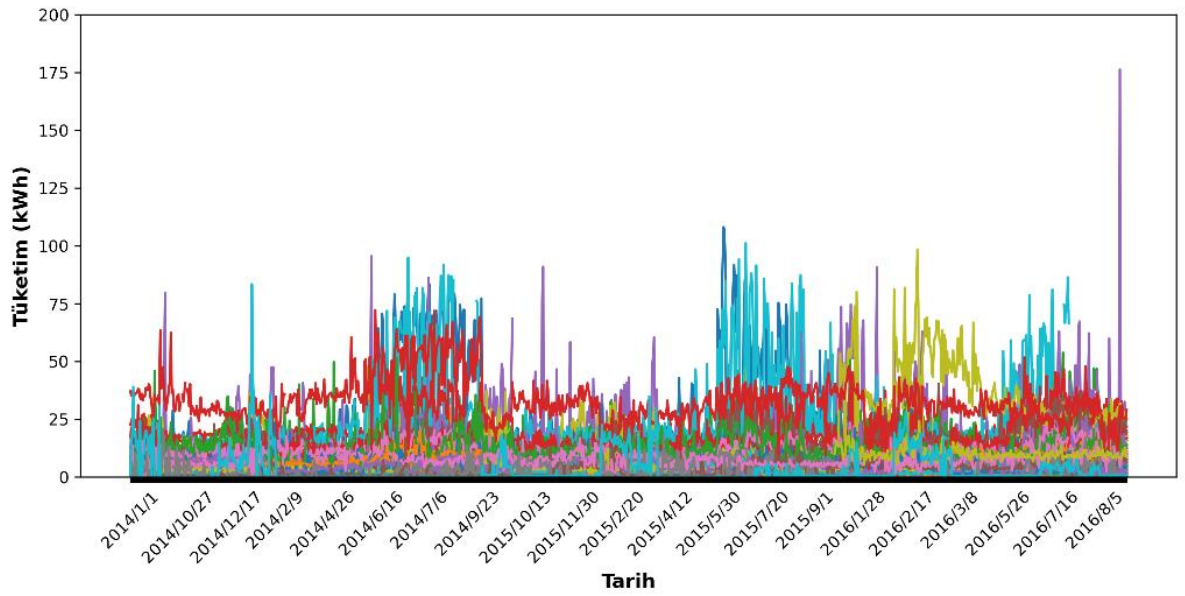

Şekil 1. Yasal kullanım sınıfına ilişkin 100 adet örnek veri.

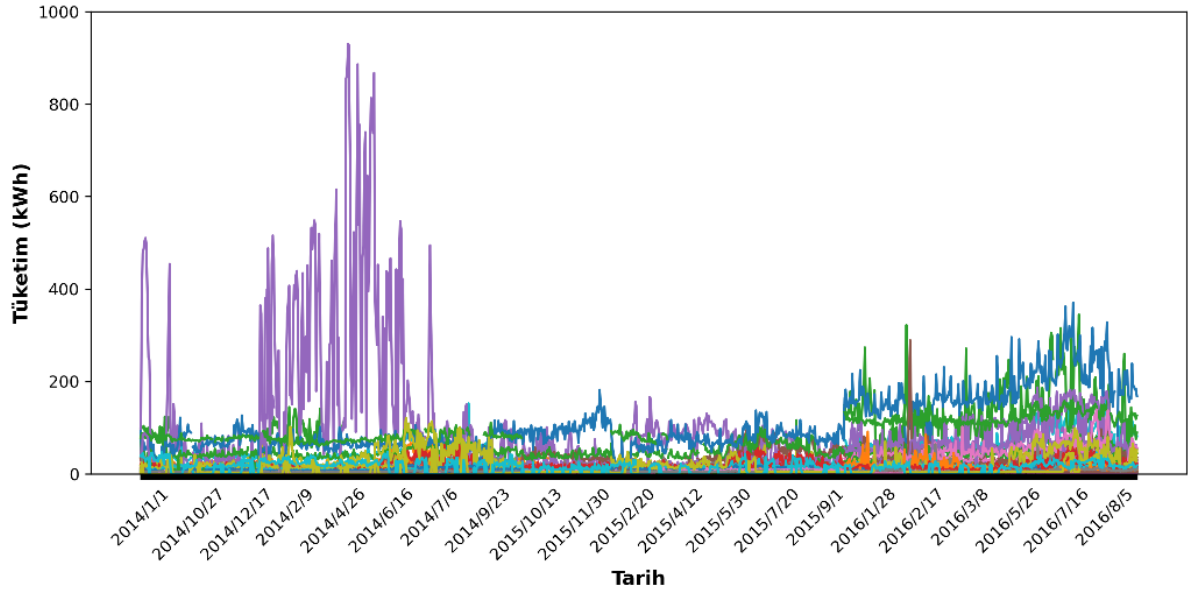

Şekil 2. Kaçak kullanım sınıfına ilişkin 100 adet örnek veri.

2.2. Ele alınan makine öğrenmesi modelleri

Eldeki veri kümesinin özellikleri (eksik ve dengesiz veri koşulları) göz önüne alındığında, gradyan artırmalı karar ağacı (gradient boosting decision trees – GBDT) tabanlı makine öğrenmesi modellerinin, problemin çözümünde etkin olacağı düşünülmüştür. GBDT tabanlı modeller, eksik veri varlığında dahi eğitilebilmekte ve veri doldurma yöntemlerine gerek duymamaktadır [31]. Ayrıca yapılan deneysel çalışmalar, GBDT tabanlı modellerin dengesiz veri koşullarında yüksek başarım sağladığını göstermiştir [32].

GBDT tabanlı yöntemler, birer topluluk öğrenme (ensemble learning) modelidir [33]**.** Bu modellerde, karar ağacı tabanlı pek çok "zayıf öğrenici" eğitilir. Eğitim algoritmasının temel mantığı, öğrenicilerin hatalarına odaklanılarak topluluğa yeni karar ağaçlarının eklenmesine dayanır. Özellikle, topluluktaki her yeni ağaç, önceki ağaçların artıkları (yani, tahmin edilen ve gerçek değerler arasındaki farklar) üzerinde eğitilir. Eğitim sonunda elde edilen GBDT tabanlı modelin nihai tahmini, topluluktaki tüm ağaçların tahminlerinin bir kombinasyonu olur.

Literatürde pek çok farklı GBDT tabanlı makine öğrenmesi modeli önerilmiştir. Bu çalışmada, bu modellerden üç tanesi ele alınmıştır. Bunlar, Microsoft tarafından geliştirilen LightGBM [34], Chen ve Guestrin tarafından önerilen XGBoost [35] ve Yandex tarafından geliştirilen CatBoost [36] modelleridir.

2.3. Model eğitimi ve üstparametre optimizasyonu

Makine öğrenmesi modellerinin eğitimi için, eldeki veri kümesinin %80'i eğitim kümesi olarak alınmış, geri kalan %20'lik bölümü sınama kümesi olarak ayrılmıştır. Model eğitimine geçilmeden önce, model başarımını önemli ölçüde etkileyen üstparametre (hyperparameter) değerlerine karar verilmesi gerekmektedir. Bu amaçla, her bir model için üç ayrı üstparametre ele alınmış ve bunlar için ayrık ve sonlu bir üstparametre uzayı oluşturulmuştur (bkz. Tablo 2).

Tablo 2. Ele alınan üstparametreler ve üstparametre uzayları.

Model	Üstparametre 1	Üstparametre 1 uzayı	Üstparametre 2	Üstparametre 2 uzayı	Üstparametre 3	Üstparametre 3 uzayı
LightGBM	max_depth	{4, 8, 16}	num_leaves	{8, 16, 32}	class_weight	{1, 5, 10, 15}
XGBoost	max_depth	{4, 8, 16}	eta	{0,1, 0,3, 0,5}	scale_pos_weight	{1, 5, 10, 15}
CatBoost	max_depth	{4, 6, 8}	learning_rate	{0,03, 0,05, 0,1}	scale_pos_weight	{1, 5, 10, 15}

Tablo 2'de verilen "max_depth", karar ağacı derinliği için, "num_leaves" ise ağaçlardaki yaprak sayısı için bir üst sınır belirler. Bu değerler model karmaşıklığını düzenler. Öte yandan, "eta" ve "learning_rate", öğrenme hızını belirlemektedir. Yüksek öğrenim hızı, eğitim sürecini hızlandırabilir ancak başarımı düşürebilir. Son olarak LightGBM için "class_weight" ve XGBoost ile CatBoost için "scale_pos_weight" üstparametreleri, az sayıda örnek içeren sınıfa (yani, kaçak kullanım sınıfına) bir ağırlık değeri atayarak, var olan veri dengesizliği durumunun yarattığı başarım düşümünü bertaraf etme amacıyla kullanılmaktadır.

Oluşturulan üstparametre uzayında, eğitim kümesinin %20'si kullanılmış ve ayırma geçerlemesi (hold-out validation) ile ızgara arama (grid search) yöntemi kullanılarak optimizasyon gerçekleştirilmiştir. Tablo 2'de görüldüğü üzere, her bir makine öğrenmesi modeli için, her biri farklı üstparametre kombinasyonu içeren 36'şar adet aday model söz konusudur. Bu aday modeller, farklı başarım ölçevleri kullanılarak sınanmış ve en iyi ölçev değerlerini veren aday modeller "nihai model" olarak alınmıştır. Bu amaçla ele alınan başarım ölçevleri, Kısım 2.4'te ifade edilmiştir.

2.4. Başarım denetleme ölçevleri

Bu çalışmada, sınıflandırıcıların başarımlarının denetlenmesi için üç ayrı başarım ölçevi ele alınmıştır. Bunlar, doğruluk (accuracy), duyarlılık (recall) ve AUC (ROC eğrisi altında kalan alan – Area Under the ROC Curve) olarak belirlenmiştir. Her üç ölçev de 0 ile 1 arası değer alır ve daha yüksek değerler daha iyi başarımı gösterir.

Doğruluk ve duyarlılık değerleri, sırasıyla (1) ve (2) 'de verilen ifadeler ile hesaplanabilir:

$$Doğruluk = \frac{DY + DK}{DY + DK + YY + YK} \tag{1}$$

$$Duyarlılık = \frac{DK}{DK + YY} \tag{2}$$

Burada DY ve DK, sırasıyla doğru olarak tahmin edilmiş yasal ve kaçak kullanımları; YY ve YK ise sırasıyla yanlış olarak tahmin edilmiş yasal ve kaçak kullanımları ifade etmektedir. AUC ölçevi ise, ROC (Receiver Operating Characteristic – alıcı işletim karakteristiği) eğrisi altında kalan alanı ifade eder. ROC eğrisi, doğru pozitif oranı ve yanlış pozitif oranı arasındaki ilişkiyi tarifleyen bir eğridir. AUC ise, ROC eğrisi çizildikten sonra sayısal integrasyon yöntemleri ile hesaplanır.

Çalışma kapsamında model geliştirme ve sınama süreçlerinde izlenen metodoloji, Şekil 3'te verilen akış şeması ile özetlenmiştir.

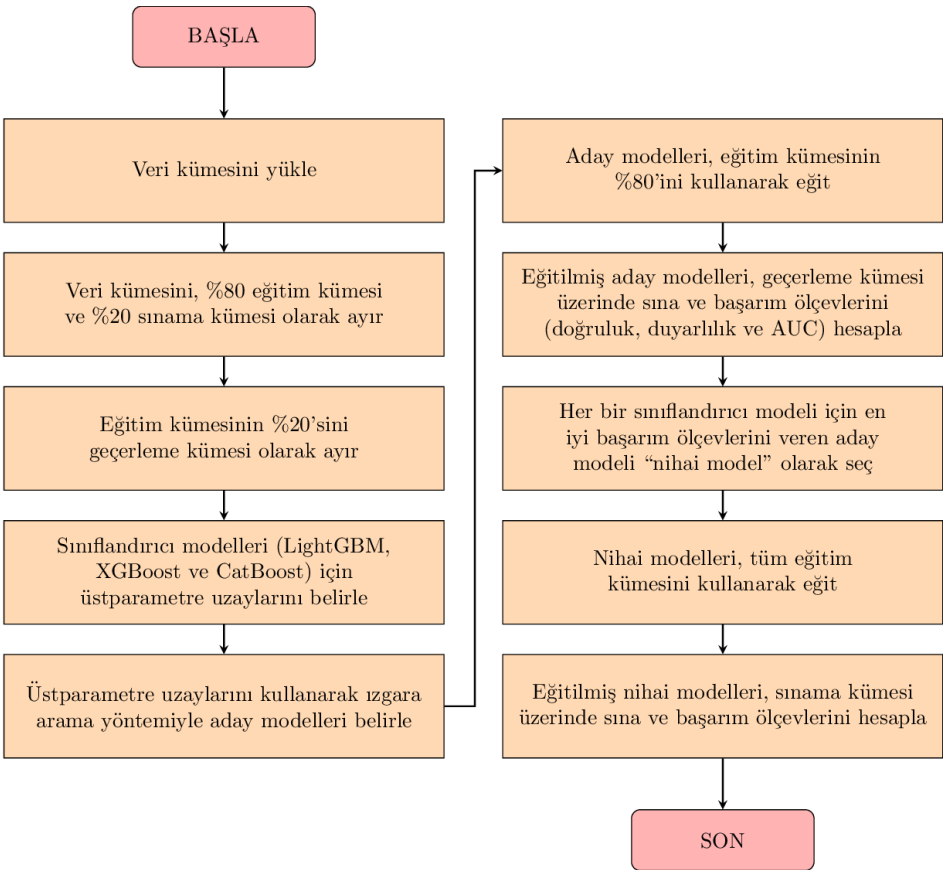

Şekil 3. Model geliştirme ve sınama metodolojisine ilişkin akış şeması.

3. Bulgular

Bu kısımda, üstparametre optimizasyonu süreci ile edinilen aday model başarım değerleri, seçilen nihai modeller ve bu nihai modellerin sınama kümesi üzerindeki başarımları gösterilmiştir. Model geliştirme süreçleri Python ortamında pandas, numpy, scikit-learn, lightgbm, xgboost ve catboost kütüphaneleri kullanılarak gerçekleştirilmiştir.

3.1. Üstparametre optimizasyonu bulguları

LightGBM, XGBoost ve CatBoost için farklı üst parametre değerleri üzerinden oluşturulan 36'şar adet aday modelin, önceki kısımda ifade edilen başarım ölçevleri kullanılarak elde edilen geçerleme sonuçları, sırasıyla Şekil 4, 5 ve 6'da verilmiştir. Aday modeller, duyarlılık ölçevine göre azalan şekilde sıralanmıştır.

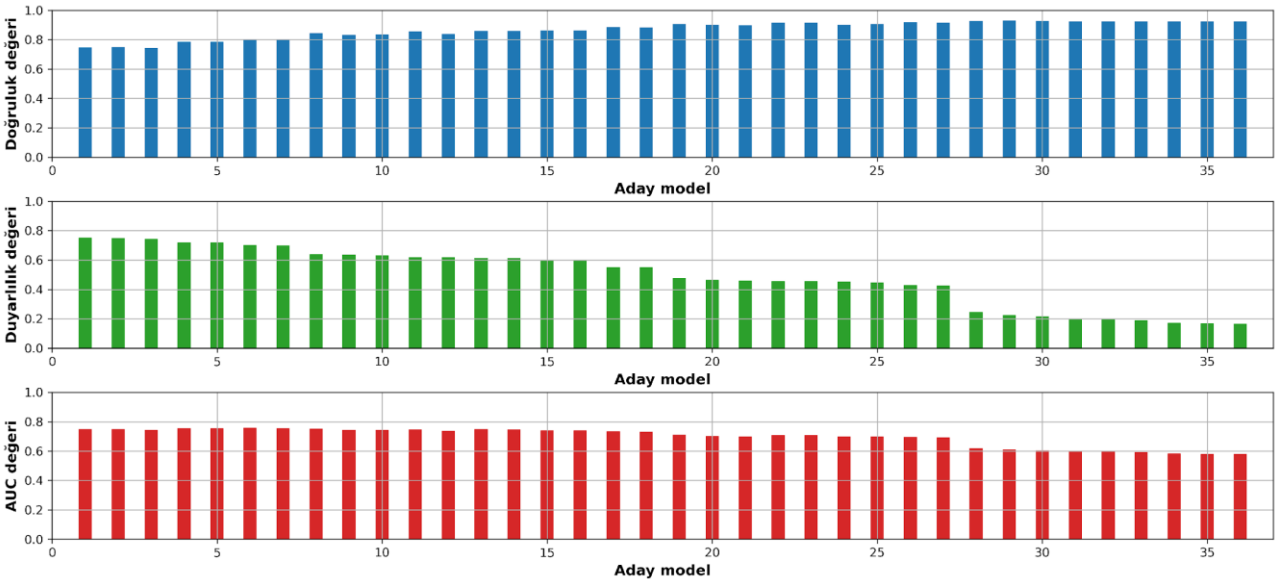

Şekil 4. LightGBM aday modelleri için geçerleme sonuçları.

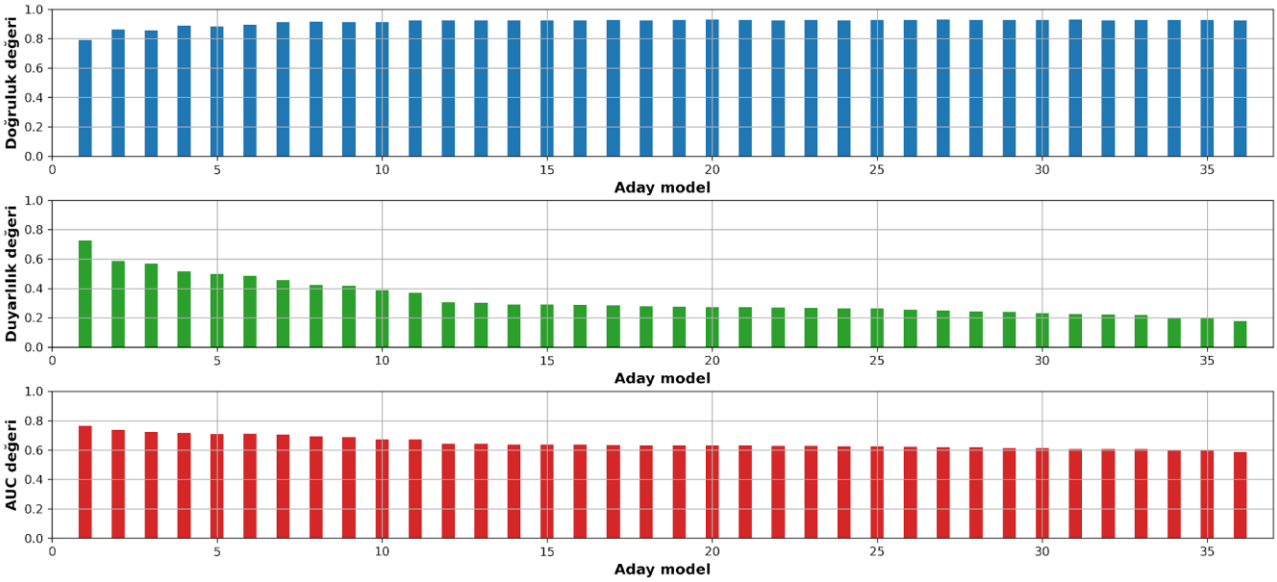

Şekil 5. XGBoost aday modelleri için geçerleme sonuçları.

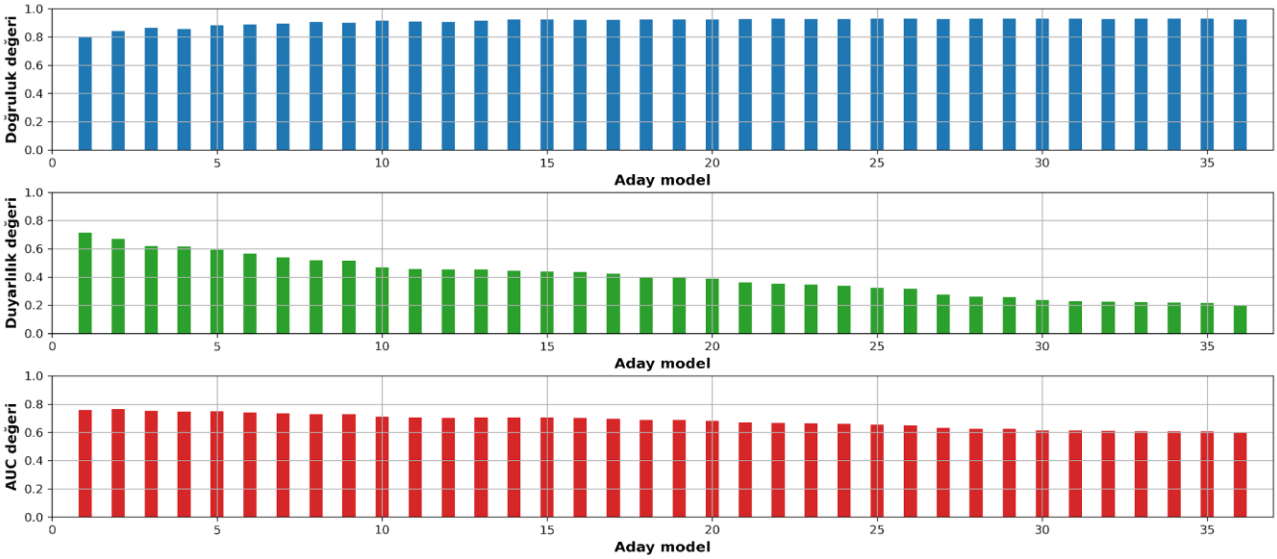

Şekil 6. CatBoost aday modelleri için geçerleme sonuçları.

Verilen grafiklere bakıldığında, aynı model için farklı üstparametrelerin kullanılması, başarım değerlerini %70'e varan mertebelerde değiştirmektedir. Bu da üstparametre optimizasyonunun önemini göstermektedir. Söz konusu veriler incelendiğinde, LightGBM, XGBoost ve CatBoost için 1 numaralı aday modellerin, her üç başarı ölçevi de düşünüldüğünde, uygun ve dengeli başarım değerlerini verdiği sonucuna varılmış ve bu aday modellerin nihai model olarak alınmasına karar verilmiştir. Seçilen nihai modeller için geçerleme sonuçları ile ilgili çeşitli detaylar, Tablo 3'te sunulmuştur.

Tablo 3. Seçilen nihai modeller için geçerleme sonuçları
(en iyi değerler, kalın italik olarak verilmiştir).

Model	Üstparametre 1 değeri	Üstparametre 2 değeri	Üstparametre 3 değeri	Doğruluk	Duyarlılık	AUC
LightGBM	4	8	15	%74,65	***%75,26***	%74,92
XGBoost	4	0,1	15	%79,26	%72,66	***%76,27***
CatBoost	4	0,03	15	***%79,48***	%71,45	%75,84

Tablo 3'teki veriler incelendiğinde, doğruluk ölçevinde CatBoost, duyarlılık ölçevinde LightGBM ve AUC ölçevinde ise XGBoost modelinin en yüksek başarım değerini verdiği görülebilir. Bununla beraber, nihai modellerin başarımları, modellerin tüm eğitim kümesinde eğitilmesi sonrası sınama kümesi üzerinde sınanması ile bir sonraki kısımda verilmiştir.

3.2. Sınama kümesi üzerinde başarım denetleme

Elde edilen nihai modeller, üstparametre optimizasyonu ve eğitim süreçlerinde kullanılmayan %20'lik sınama kümesi üzerinde sınanmış ve başarımları denetlenmiştir. Gözlemlenen başarım ölçevi değerleri ve modellerin eğitim süreleri, Tablo 4'te sunulmuştur.

Tablo 4. Nihai modeller için sınama kümesi üzerinde elde edilen değerler
(en iyi değerler, kalın italik olarak verilmiştir)

Model	Doğruluk	Duyarlılık	AUC	Eğitim süresi (sn.)
LightGBM	%73,49	***%72,48***	%73,02	***4,38***
XGBoost	%77,71	%68,88	%73,70	37,79
CatBoost	***%78,10***	%69,43	***%74,17***	66,20

Verilere bakıldığında, CatBoost tabanlı sınıflandırıcı modelinin doğruluk ve AUC ölçevinde de diğer iki modelden daha yüksek değerler elde ettiği görülebilir. CatBoost diğer modellere, doğruluk ölçevinde 4,61 puan ve AUC ölçevinde 1,15 puana varan bir üstünlük sağlamıştır. Duyarlılık ölçevinde ise en iyi değere LightGBM modeli ulaşmıştır.

Ele alınan ölçevlerde CatBoost modelinin başarımı öne çıksa da bu model uzun eğitim süresi ile göze çarpmaktadır. LightGBM'in yaklaşık 15 katı bir işlem süresi yükü olan CatBoost eğitiminin, milyonlarca örnek içeren bir veri kümesi varlığında günler sürebileceği tahmin edilebilir. Bu durumda GPU tabanlı eğitim yapılabilir veya daha az işlem yükü olan LightGBM modeli tercih edilebilir. Son olarak, her üç model için de elde edilen doğruluk matrisleri Şekil 7'de, ROC eğrileri ise Şekil 8'de verilmiştir.

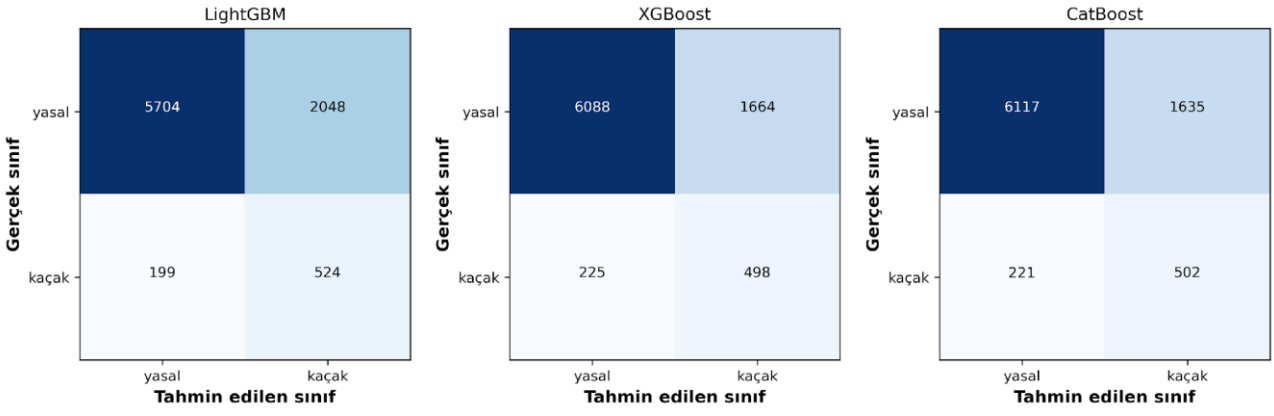

Şekil 7. Nihai modeler için sınama kümesi üzerinde elde edilen doğruluk matrisleri.

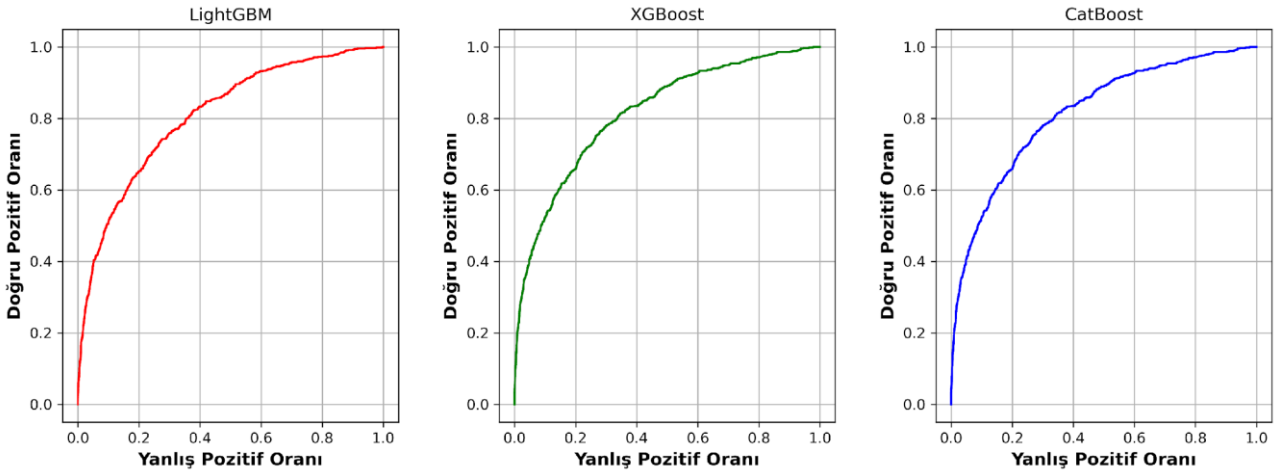

Şekil 8. Nihai modeler için sınama kümesi üzerinde elde edilen ROC eğrileri.

Elde edilen bulgulardan hareketle, her üç model kullanılarak elde edilen başarım değerlerinin, özellikle veri kümesinde yaklaşık 1/4 değerindeki eksik veri ve 1/10 değerindeki veri dengesizliği oranları da düşünüldüğünde, kaçak elektrik kullanımlarının tespiti için uygun nitelikte olduğu değerlendirilebilir. Enerji dağıtım şirketleri, bu modelleri kullanarak kaçak elektrik kullanım şüphesi bulunan tüketicileri tespit edebilir, daha sonra sayaç ve tesisat incelemesi gibi işlemleri başlatıp kaçak elektrik kullanımının var olup olmadığı konusunda nihai karara varabilir. Bu sayede, hem milyonlarca tüketiciden elde edilen yüksek boyutlu verilerin analizi otomatikleştirilerek insan gücü kaynağı etkin kullanılmış, hem de kaçak elektrik kullanımından doğan ekonomik ve sosyal kayıplar en aza indirilmiş olur.

4. Tartışma ve Sonuç

Bu çalışmada, tüketicilerde kaçak elektrik kullanımının akıllı sayaçlardan alınan tarihsel günlük elektrik tüketimi verilerine dayalı olarak tespiti için üç farklı gradyan artırmalı karar ağacı tabanlı makine öğrenmesi sınıflandırıcı modeli önerilmiştir. Ele alınan modeller olan LightGBM, XGBoost ve CatBoost sınıflandırıcılarının üstparametreleri optimize edilmiş, bu süreçte hesaplanan üç farklı başarım ölçevi değerleri göz önüne alınarak birer nihai model elde edilmiştir.

Nihai modeler kullanılarak sınama kümesinde yapılan başarım denetleme çalışmalarında, CatBoost tabanlı sınıflandırıcı modelinin doğruluk ve AUC ölçevlerinde sırasıyla %78,10 ve %74,17 değerleri ile, LightGBM modelinin ise duyarlılık ölçevinde %72,48 değeri ve 4,38 saniyelik eğitim süresi ile diğer modellere kıyasla daha yüksek başarımlı olduğu sonucuna varılmıştır. Elde edilen bulgular, akıllı sayaçlardan alınan verilerin makine öğrenmesi yöntemleri kullanılarak işlenmesiyle kaçak elektrik kullanımının yüksek doğrulukla tespit edilebileceğini gösterir niteliktedir. Bu tespit işlemi, eksik ve dengesiz veri koşullarında dahi başarıyla gerçekleştirilebilmektedir.

Gelecekte yapılacak çalışmalarda, sınıflandırma başarımının daha da artırılmasına odaklanılarak, işaret işleme tabanlı veri önişleme yöntemleri, dengesiz veri durumunun üstesinden gelmek için aşırı örnekleme yöntemleri ve birden fazla makine öğrenmesi modelinin bir araya getirilmesiyle oluşturulacak topluluk modelleri gibi yaklaşımlar kullanılacaktır. Dünya genelinde kullanımı giderek artan akıllı sayaç teknolojisinin ülkemizde de yaygınlaşmasıyla beraber, toplumun her kesimini maddi manevi kayba uğratan kaçak elektrik kullanımının düşürülmesinde önemli rol oynayacağına inanıyoruz.

Teşekkür

Bu çalışma T.C. Sanayi ve Teknoloji Bakanlığı tarafından AGTMPR94340 no'lu proje ile desteklenmiştir. Çalışma boyunca desteklerini esirgemeyen Çözümevi Ar-Ge Merkezi Direktörü Sn. Hakan Çolak, Çözümevi Ar-Ge Merkezi Araştırmacıları Sn. Şükran Batur, Sn. Mustafa Özkan ve Sn. Burak Müderrisoğlu'na ve tüm Çözümevi Yönetim Danışmanlığı ve Bilgisayar Yazılım Ticaret A.Ş. ailesine teşekkürlerimizi sunarız.

Yazar Katkı Oranları

Y. Kara – Fikir, tasarım, denetleme, kaynaklar, veri toplama/işleme, analiz, literatür tarama, yazım, eleştirel inceleme. A. Aksu – fikir, tasarım, denetleme, kaynaklar, yazım, eleştirel inceleme.

Çıkar Çatışması

Tüm yazarlar, Çözümevi Yönetim Danışmanlığı ve Bilgisayar Yazılım Ticaret A.Ş. firmasında çalışmaktadır.

Kaynakça

[1] de Souza Savian, F., Siluk, J. C. M., Garlet, T. B., do Nascimento, F. M., Pinheiro, J. R., & Vale, Z. (2021). Non-technical losses: A systematic contemporary article review. *Renewable and Sustainable Energy Reviews*, 147, 111205.

[2] Enerji Piyasası Düzenleme Kurumu (EPDK). (2022). Güncel 6446 Sayılı Elektrik Piyasası Kanunu. https://www.epdk.gov.tr/Detay/Icerik/3-14650/guncel-6446-sayili-elektrik-piyasasi-kanunu (Erişim tarihi: 01.04.2023).

[3] Yıldız, E., & Çetinkaya, N. (2022). Elektrik güç sistemlerindeki kaçak kullanımların yapay sinir ağları ile tahmini. *Journal of Investigations on Engineering and Technology*, 5(1), 1-10.

[4] Biswas, P. P., Cai, H., Zhou, B., Chen, B., Mashima, D., & Zheng, V. W. (2019). Electricity theft pinpointing through correlation analysis of master and individual meter readings. *IEEE Transactions on Smart Grid*, 11(4), 3031-3042.

[5] Türkiye Elektrik Dağıtım Anonim Şirketi (TEDAŞ). (2020). 2020 Yılı Türkiye Elektrik Dağıtımı Sektör Raporu. https://www.tedas.gov.tr/sx.web.docs /tedas/docs/Stratejikplan/2020_Yili_Turkiye_Elektrik_Dagitimi_Sektor_Raporu.pdf (Erişim tarihi: 01.04.2023).

[6] T.C. Hakkari Valiliği. (2020). İlimiz Türkiye Genelinde Kaçak Elektriğin En Çok Kullanıldığı İlk 5 il arasında Yer Alıyor. http://www.hakkari.gov.tr/ilimiz-turkiye-genelinde-kacak-elektrigin-en-cok-kullanildigi-ilk-5-il-arasinda-yer-aliyor (Erişim tarihi: 01.04.2023).

[7] Hasan, M. N., Toma, R. N., Nahid, A. A., Islam, M. M., & Kim, J. M. (2019). Electricity theft detection in smart grid systems: A CNN-LSTM based approach. *Energies*, 12(17), 3310.

[8] Leite, J. B., & Mantovani, J. R. S. (2016). Detecting and locating non-technical losses in modern distribution networks. *IEEE Transactions on Smart Grid*, 9(2), 1023-1032.

[9] Haq, E. U., Pei, C., Zhang, R., Jianjun, H., & Ahmad, F. (2023). Electricity-theft detection for smart grid security using smart meter data: A deep-CNN based approach. *Energy Reports*, 9, 634-643.

[10] Mertoğlu, Z., & Tezcan, S. S. (2019). Kaçak Elektrik Kullanımının Enterkonnekte Sisteme Etkileri. *El-Cezeri*, 6(3), 571-584.

[11] Otuoze, A. O., Mustafa, M. W., Abioye, A. E., Sultana, U., Usman, A. M., Ibrahim, O., ... & Abu-Saeed, A. (2022). A rule-based model for electricity theft prevention in advanced metering infrastructure. *Journal of Electrical Systems and Information Technology*, 9(1), 1-17.

[12] Kocaman, B. (2018). Teknik Olmayan Enerji Kayıplarının Azaltılmasında PLC Sayaçlarının Önemi. *Bitlis Eren Üniversitesi Fen Bilimleri Dergisi*, 7(2), 220-230.

[13] Yan, Z., & Wen, H. (2021). Performance analysis of electricity theft detection for the smart grid: An overview. *IEEE Transactions on Instrumentation and Measurement*, 71, 1-28.

[14] Huang, Y., & Xu, Q. (2021). Electricity theft detection based on stacked sparse denoising autoencoder. *International Journal of Electrical Power & Energy Systems*, 125, 106448.

[15] Adil, M., Javaid, N., Qasim, U., Ullah, I., Shafiq, M., & Choi, J. G. (2020). LSTM and bat-based RUSBoost approach for electricity theft detection. *Applied Sciences*, 10(12), 4378.

[16] Lepolesa, L. J., Achari, S., & Cheng, L. (2022). Electricity theft detection in smart grids based on deep neural network. *IEEE Access*, 10, 39638-39655.

[17] Pereira, J., & Saraiva, F. (2021). Convolutional neural network applied to detect electricity theft: A comparative study on unbalanced data handling techniques. *International Journal of Electrical Power & Energy Systems*, 131, 107085.

[18] Lin, G., Feng, H., Feng, X., Wen, H., Li, Y., Hong, S., & Ni, Z. (2021). Electricity theft detection in power consumption data based on adaptive tuning recurrent neural network. *Frontiers in Energy Research*, 9, 773805.

[19] Tehrani, S. O., Moghaddam, M. H. Y., & Asadi, M. (2020, September). Decision tree based electricity theft detection in smart grid. In *2020 4th International conference on smart city, internet of things and applications (SCIOT)* (pp. 46-51). IEEE.

[20] Li, S., Han, Y., Yao, X., Yingchen, S., Wang, J., & Zhao, Q. (2019). Electricity theft detection in power grids with deep learning and random forests. *Journal of Electrical and Computer Engineering*, 2019, 1-12.

[21] Toma, R. N., Hasan, M. N., Nahid, A. A., & Li, B. (2019, May). Electricity theft detection to reduce non-technical loss using support vector machine in smart grid. In *2019 1st International Conference on Advances in Science, Engineering and Robotics Technology (ICASERT)* (pp. 1-6). IEEE.

[22] Aslam, Z., Ahmed, F., Almogren, A., Shafiq, M., Zuair, M., & Javaid, N. (2020). An attention guided semi-supervised learning mechanism to detect electricity frauds in the distribution systems. *IEEE Access*, 8, 221767-221782.

[23] Lu, X., Zhou, Y., Wang, Z., Yi, Y., Feng, L., & Wang, F. (2019). Knowledge embedded semi-supervised deep learning for detecting non-technical losses in the smart grid. *Energies*, 12(18), 3452.

[24] Boucetta, C., Flauzac, O., Nassour, A. N. M., & Nolot, F. (2020, June). Multi-level Hierarchical Clustering Algorithm For Energy-theft Detection in Smart Grid Networks. In *2020 International Conference on Electrical, Communication, and Computer Engineering (ICECCE)* (pp. 1-6). IEEE.

[25] Lin, Q., Li, M., Feng, S., Yang, J., Surn, X., Li, J., ... & Xie, X. (2022, September). Identification of electricity theft based on the k-means clustering method. In *2022 IEEE 9th International Conference on Power Electronics Systems and Applications (PESA)* (pp. 1-6). IEEE.

[26] Zheng, Z., Yang, Y., Niu, X., Dai, H. N., & Zhou, Y. (2017). Wide and deep convolutional neural networks for electricity-theft detection to secure smart grids. *IEEE Trans. on Industrial Informatics*, 14(4), 1606-1615.

[27] State Grid Cooperation of China. (2023). http://www.sgcc.com.cn/ (Erişim tarihi: 01.04.2023).

[28] henryRDlab. (2018). https://github.com/henryRDlab/ElectricityTheftDetection (Erişim tarihi: 01.04.2023).

[29] Emmanuel, T., Maupong, T., Mpoeleng, D., Semong, T., Mphago, B., & Tabona, O. (2021). A survey on missing data in machine learning. *Journal of Big Data*, 8(1), 1-37.

[30] Chawla, N. V., Bowyer, K. W., Hall, L. O., & Kegelmeyer, W. P. (2002). SMOTE: synthetic minority over-sampling technique. *Journal of Artificial Intelligence Research*, 16, 321-357.

[31] Aydin, Z. E., & Ozturk, Z. K. (2021). Performance analysis of XGBoost classifier with missing data. *Manchester Journal of Artificial Intelligence and Applied Sciences (MJAIAS)*, 2(02), 2021.

[32] Brown, I., & Mues, C. (2012). An experimental comparison of classification algorithms for imbalanced credit scoring data sets. *Expert Systems with Applications*, 39(3), 3446-3453.

[33] Friedman, J. H. (2001). Greedy function approximation: a gradient boosting machine. *Annals of Statistics*, 1189-1232.

[34] Ke, G., Meng, Q., Finley, T., Wang, T., Chen, W., Ma, W., ... & Liu, T. Y. (2017). LightGBM: A highly efficient gradient boosting decision tree. *Advances in Neural Information Processing Systems*, 30.

[35] Chen, T., & Guestrin, C. (2016, August). XGBoost: A scalable tree boosting system. In *Proceedings of the 22nd ACM SIGKDD International Conference on Knowledge Discovery and Data Mining* (pp. 785-794).

[36] Prokhorenkova, L., Gusev, G., Vorobev, A., Dorogush, A. V., & Gulin, A. (2018). CatBoost: unbiased boosting with categorical features. *Advances in Neural Information Processing Systems*, 31.

Journal of Investigations on Engineering & Technology
Volume 6, Issue 1, 13-27, 2023

ISSN: 2687-3052

Research Article

MHD Nanofluidic Flow Past a Nonlinear Exponentially Stretched Plate with Enhanced Thermal Source/Sink and Thermo-migration

Uchenna A. UKA[1], Digbo I. IKU[2], Great E. ESEKHAIGBE[3]

(Received: 26.04.2023, Accepted: 13.07.2023, Published Online: 26.07.2023)

Keywords

Metallic Particles
Nanofluidics
Ordinary Differential Equations
Series Approximation Scheme
Wolfram Mathematica

Abstract: The study investigates the heat transfer characteristics of a nanofluidic flow past a non-linear exponentially stretched plate in the presence of enriched heat generation/absorption through the application of the Standard series approximation technique. The significance of the study includes but is not limited to drug targeting, food processing industries, manufacturing firms, solar power technology and nuclear mechanizations etc. The mathematical models governing the fluid flow was modelled through the Navier-Stokes equations. Thus, such partial differential expressions (PDE) were transformed into coupled ordinary differential models (CODM) through the application of adequate similarity transformation variables. Thereafter, the resulting equations were solved by the use of the aforementioned technique with appropriate boundary conditions. However, the Wolfram Mathematica package has been applied for the numerical solutions. Thus, the results showed that the presence of nanoparticles and thermal source/sink significantly affects the velocity, temperature and mass concentration. It was found that an increase in the Hartman number leads to a decline in the velocity of the flow whereas the velocity distribution surges as radiation and Grashof parameters appreciate in values. Similarly, a rise in the thermo-migration factor breeds an upsurge in temperature and nanoparticle concentration respectively. The results also showed that an improvement in the values of Prandtl and Schmidt numbers led to a reduction in the thermal and mass boundary layer thicknesses. Therefore, this study provides an insight into the heat transfer characteristics of nanofluidic flow and can be used in various engineering applications such as cooling of electronic devices and nuclear reactors.

1. Introduction

Magnetohydrodynamics is the study of the motion of electrically conducting fluids in the presence of magnetic fields. Recently, the studies of heat transfer in nanofluidics have attracted the interest of many scholars due to its significance in the area of technological advancement. However, this type of fluids consist of colloidal immersions of finely divided nanoparticles of metals and their oxides, and etc. in a base fluid such as water,

[1] Uchenna A. Uka 1 Babcock University, School of Science and Engineering, Basic Science Department, 121003, Ilishan-Remo, Ikenne, Nigeria.
[2] Digbo I. Iku 2 Babcock University, School of Science and Engineering, Basic Science Department, 121003, Ilishan-Remo, Ikenne, Nigeria.
[3] Great E. Esekhaigbe 3 University of Africa, Department of Mathematics and Computer Science, 561101, Bayelsa State, Nigeria.

Corresponding Author and e–mail address: Uchenna A. Uka ukau@babcock.edu.ng

engine oil, etc. and have appeared as a capable alternative to conventional coolants due to their unique properties that make them suitable for many industrial applications and in the radiator of an automobile system. Often, a surface-active agent like a 'surfactant' is being added in order to maintain the composition's stability and reduces surface tension, thereby improving its thermal conductivity. Meanwhile, their application in such system has the prospective of reducing the negative environmental impacts. This is because the traditional coolants such as ethylene glycol (EG) and propylene glycol usually comprise harmful chemicals, which can pose dangers to human health and the environment. Conversely, nanofluids tend to be environmentally friendly by decreasing the negative effects linked with coolant discarding and leakage. Thus, scientifically nanofluids remain the best for refining the performance and sustainability of automobile cooling systems. Hence, the thermal conductivity of the nanofluid is enhanced

Sharma et al., [1] investigated MHD slip flow and temperature transference along an exponentially extending leaky piece fixed in a spongy material. Mahdi et al. [2] reviewed nanofluid flow and heat transfer passing through porous media. They laid emphasis on thermo-physical properties of the nanofluid and the form of the convective heat transfer. Rashidi et al. [3] analyzed the buoyancy effect on MHD flow of Nanofluid over a stretching sheet in the presence of thermal radiation. Mustafa et al. [4] investigated stagnation spot flow of nanofluids along an extending sheet while an analysis involving exploration of thermal transmission developments with viscous fluid flow over enlarging sheet in the presence of power law velocity distribution and nonlinear expanding proportion is conducted [5]. Miklavcic and Wang [6] reported the viscous flow over a shrinking sheet with suction effect at the boundary. They opined that the vorticity of the lessening sheet is unrestricted within a boundary layer. However, Uka et al. [7] explored chemical reaction and radiation impact on MHD Nanofluid flow over an exponentially widening sheet. From the results of their work inferred that a rise in the stretching and radiation parameters lead to an enhancement of the velocity. The analyses of heat and mass transfer with applications have been investigated by many researchers [8, 9]. Furthermore, Mansour et al. [10] affirmed the applications of heat and mass transport on magneto-hydrodynamic stream. They found out that the micro polar fluids exhibited a reduction in strain with heat transfer rate in comparison with Newtonian fluids. The first investigation of improving thermal conductivity of fluids containing nanoadditives was done by Choi and Eastman [11]. Hence, due to the overall scientific significance of nanofluid in terms of heat transmission on MHD flow, various theories have been propounded. Thus, Boungiorno [12] analyzed different theories surrounding the transferal of heat and mass in nanofluids. He considered some mechanisms that can produce a relative velocity between the nanoparticles and base fluid by testing the validity of the assumptions in his study. Similarly, the analysis of a convective nanofluid over a vertical sheet was conducted by Kuznetsov and Nield [13]. From their result, it was noted that Schmidt number wielded an obvious effect on the heat and fluid flow machinery around the exterior sphere involving velocity, temperature, and concentration distributions. The study of boundary layer flow past a continuous rigid surface with stable speed due to the fluid's movement in the surrounding area was facilitated by Sakiadios [14]. The effect of free and forced convection with Jeffery fluid in the presence of a non-isothermal segment was studied by Gaffar et al. [15]. The investigation of heat transmission in a fluid flow surrounded by a penetrable medium was carried out by Tamayol et al. [16]. According to Khani et al. [17] the examination of fluid flow in a soaking non-Darcy porous media under thermal transportation is determined. Consequently, Hayat et al. [18] presented unsteady 3-D movement of combined pressure fluid over a stretching surface with chemical reaction impact. They noted that the concentration field is a decreasing function of Schmidt number and shows opposite results for destructive $(\gamma > 0)$ and generative $(\gamma < 0)$ chemical reactions. Similarly, Awucha and Okechukwu [19] maintained that the rate at which energy flows is of paramount concern and importance due to its numerous industrial applications in the areas of cooling of nuclear reactors, power generating gadgets as well as its mechanisms. The examination of nonlinear unsteady MHD viscous, incompressible fluid distribution over an upright permeable medium due to thermal radiation and chemical reaction [20] was undertaken. The dual term perturbation approach was deployed in the solution of the problem. It was found that velocity shrinks as chemical reaction number rises. The hall current impact on the MHD stream of Newtonian fluid over a spongy channel was considered [21]. It was observed that the resultant velocity enhances as the Reynolds number improves. The influence of thermal source on mixed convection stream in nanofluids past a horizontal spherical cylinder [22] was discussed. The solutions were achieved by applying the Keller-box technique. The result showed that velocity distribution enhances and temperature distribution declines with the enhancement of the mixed convection factor.

It is important to mention that the importance of the current study applies to nuclear power machines, earth (soil) sciences, cooling of electronics, industrial metal processing, coating of cables and fibers, aerodynamic extrusion of plastic sheets, repeated casting, rolling, annealing as well as the tinning of copper cables. This study gives a direction into the behavior of MHD nanofluids flow and thermal transmission with improved thermal source/sink and thermo-migration effects. Similarly, its findings have prospective applications in designing of microfluidic devices and in the optimization of industrial processes which involve the stream of electrically conducting fluids. It is also viable in contributing to the growing body of knowledge in the field of fluid

mechanics and MHD nanofluidic drifts and provides a better understanding of the complex physics involved in these systems which can serve as a basis for further research in this area.

2. Formulation of the Problem, Materials and Method of Solution

A magneto-hydrodynamic nanofluid flow past an expanding exponentially plate in two dimensions $x \wedge y$ is considered. While $y-axis$, is normal to the plate $x-axis$ is horizontal to it as depicted in Figure 1.

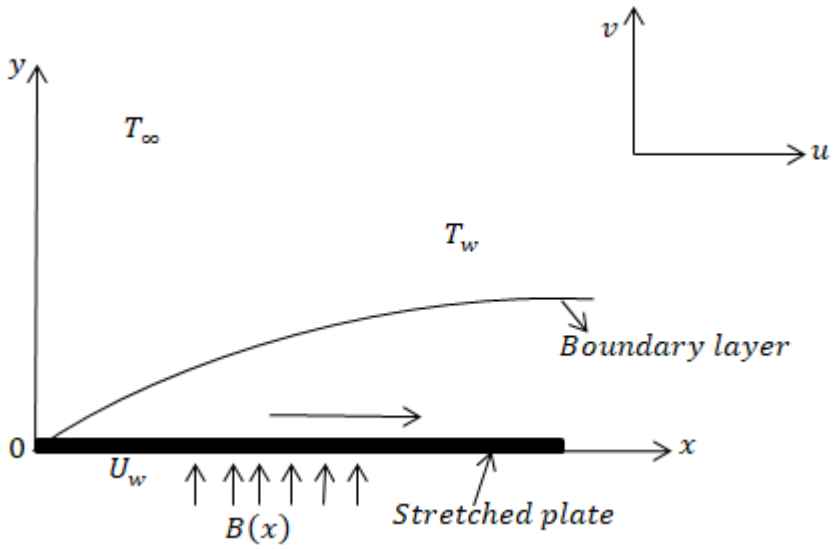

Fig. 1 Physical flow representation

The fluid flow is along the horizontal direction in such a way that the wall is expanded as the origin remains unchanged. We assume that the surface of the plate is stretched towards $x-axis$ with velocity, $U=U_w(x)=ce^{\frac{x}{l}}$. The application of a magnetic field of strength B_0^2 is also in path of $x-axis$ in such a way that the induced magnetic Reynolds factor $\mathfrak{N} \ll 1$, is of negligible value. Hence, the applied magnetic field and non-uniform heat source are considered. Therefore, the boundary layer equations are:

Continuity equation

$$\frac{\partial u}{\partial x}+\frac{\partial v}{\partial y}=0 \tag{1}$$

Momentum equation

$$u\frac{\partial u}{\partial x}+v\frac{\partial u}{\partial y}=u_\infty\frac{du_\infty}{dx}+\frac{1}{\rho}\frac{\partial}{\partial y}\left(\frac{\mu\partial u}{\partial y}\right)-\frac{\sigma B^2}{\rho}u+\frac{g\beta_T(T-T_\infty)}{v} \tag{2}$$

Energy conservation equation

$$u\frac{\partial T}{\partial x}+v\frac{\partial T}{\partial y}=\frac{k}{(\rho c)_f}\frac{\partial^2 T}{\partial y^2}+\frac{(\rho c)_p}{(\rho c)_f}\left[D_B(C-C_\infty)(T-T_\infty)+\frac{D_T}{T_\infty}(T-T_\infty)\right]-\frac{1}{(\rho c)_f}\frac{\partial q_T}{\partial y}-\frac{Q}{\rho C_p}(T-T_\infty) \tag{3}$$

Mass conservation equation

$$u\frac{\partial C}{\partial x}+v\frac{\partial C}{\partial y}=D_m\frac{\partial^2 C}{\partial y^2}+\frac{D_T}{T_\infty}\left(\frac{T-T_\infty}{T_w-T_\infty}\right)-R(C-C_\infty) \tag{4}$$

With the boundary conditions as

$$\begin{aligned} &u = U_w(x),\ \ v = -k_0,\ \ T = T_w,\ \ C = C_\infty && \text{at } y = 0 \\ &u = v \to 0,\ \ T \to T_\infty,\ C \to C_\infty && \text{as } y \to \infty \end{aligned} \tag{5}$$

with,
ρ_f =base fluid density, σ = electrical conductivity parameter, β = volumetric heat enlargement coefficient of the base fluid, g = acceleration under gravity, k = heat conduction, μ = fluid viscosity, D_T = thermophoresis diffusion coefficient, q_r = radiative heat flux, D_m = Brownian motion coefficient, Temperature, T at the boundary (y = 0) is T_w, and far from the plate is T_∞; local nanoparticle Concentration is C, $\frac{\rho c_f}{\rho c_p} = \tau$ is ratio of heat capacity of the nanofluid to nanoparticle; Q_s is heat number, and the additive inverse sign in the boundary condition above indicates that the occurrence of suction takes the same path as the plate.

We shall introduce the following variables in order to convert equations (2) – (4) into ODEs.

$$\text{Let } \eta = y\sqrt{\frac{a}{v}}e^{\frac{x}{2L}},\ \varphi = g(\eta)\sqrt{va}e^{\frac{x}{2L}},\ \theta = \frac{T-T_\infty}{T_w-T_\infty},\quad \emptyset = \frac{C-C_\infty}{C_w-C_\infty} \tag{6}$$

$$v = \frac{-\partial\varphi}{\partial x}, u = \frac{\partial\varphi}{\partial y} \tag{7}$$

Substituting equation (7) into equation (1), we obtain

$$\frac{\partial^2\varphi}{\partial x\partial y} - \frac{\partial^2\varphi}{\partial x\partial y} = 0$$

This shows that equation (1) is satisfied.

In using equations (6) and (7) to transform equations (2) – (4), we realize the following equations:

$$\begin{aligned} &g'''(\eta) + g(\eta)g''(\eta) - Hg'(\eta) + J_t\theta(\eta) = 0 \\ &(1+\tfrac{4S}{3})\theta''(\eta) + Prg(\eta)\theta'(\eta) + Nb\theta(\eta)\emptyset(\eta) + Nt\theta(\eta) + Q_s\theta(\eta) = 0 \end{aligned} \tag{8}$$

$$\emptyset''(\eta) + \frac{N_t}{N_b}\theta(\eta) + g(\eta)\emptyset'(\eta)Sc - R_cSc\emptyset(\eta) = 0 \tag{9}$$

The converted form of equation (5) follows as:

$$g(0) = g_0, g'(0) = 1, g'(\infty) = 0, \theta(0) = 1, \theta(\infty) = 0, \emptyset(0) = 1, \emptyset(\infty) = 0 \tag{10}$$

With, Hartman number $H = \frac{2\sigma B^2 L}{\rho U_W}$, local Grashof number $J_t = \frac{g\beta_T(T_W-T_\infty)l^3}{v^2}$,
Prandtl number $Pr = \frac{\mu c_p}{k}$, thermo-migration parameter $N_t = \frac{\tau D_T(T_W-T_\infty)}{T_\infty v}$, radiation term $S = \frac{4T_\infty^3\sigma}{3k\ \ k}$, Brownian diffusion parameter $N_b = \frac{\tau D_B(C_W-C_\infty)}{v}$, Schmidt number $Sc = \frac{v}{D_m}$, modified rate of chemical reaction $R_c = \frac{2Lkr}{U_W}$, heat number $Q_s = \frac{2vl\rho C_f Q_s}{kU_W}$, parameter for suction $g_0 = \frac{z_W}{\sqrt{\square}}$ and the primes relates to differentiation, $fo > 0$ implies suction at the surface of the plate while $fo < 0$ is indicative of injection or blowing. The series approximation method [23] has been proved to be reliable and efficient. The method is simple in terms of its application just as its convergent rate is faster. Meanwhile, this method is a mathematical technique used to approximate the solution to a problem that involves a small parameter. It is mainly beneficial when faced with coupled and complex equations that cannot be solved directly. The methodology involves expanding the solution as a series in powers of the small parameter and iteratively solving the resulting equations to obtain successive

approximations. The presence of a small parameter given by ϖ, quantifies the magnitude of the method. Then, the solution to the problem is assumed and can be expressed as a power series in the small parameter ϖ. i.e., Solution = $\text{Solution}_0 + \varpi\,\text{Solution}_1 + \varpi^2\,\text{Solution}_2 + \ldots$

Where Solution_0 is the zeroth-order approximation, Solution_1 entails the first-order approximation, etc. Thereafter, substitutions of the expansions into the original equation(s) are carried out. Thus, expansion of the equations and grouping of terms with similar powers of the term ϖ follow. Then, the coefficients of the same power of ϖ are equated on both sides of the expanded equations and each equation is solved separately with its transformed physical boundary constraints to obtain the solution at each order. Finally, the solutions obtained are simulated with the Wolfram Mathematica package for the realization of the numerical solutions.

In order to apply the aforementioned procedure of solution, we need to make the following definitions:

$$\text{Let } \eta = \vartheta g_0, g(\eta) = g_0 G(\eta), \theta(\eta) = \Theta(\eta), \emptyset(\eta) = \emptyset(\eta), \varpi = \frac{1}{(g_0)^2} \tag{11}$$

Such that differentiating equation (11) accordingly yields

$$\begin{aligned} &g' = (g_0)^2 G',\ g'' = (g_0)^3 G'',\ g''' = (g_0)^4 G''',\ g''' = (g_0)^4 G''',\ \theta' = g_0 \Theta', \\ &\theta'' = (g_0)^2 \Theta'', \emptyset'(\eta) = g_0 \emptyset'(\eta),, \emptyset''(\eta) = (g_0)^2 \emptyset''(\eta) \end{aligned} \tag{12}$$

By substituting equations (11) and (12) into equations (7) – (9), we have

$$G'''(\eta)(g_0)^4 + G(\eta)G''(\eta)(g_0)^4 - HG'(\eta)(g_0)^2 + J_t\Theta(\eta) = 0 \tag{13}$$

$$(1 + \frac{4S}{3})\Theta''(\eta)(g_0)^2 + PrG(\eta)\Theta'(\eta)(g_0)^2 + Nb\theta(\eta)\emptyset(\eta) + Nt\Theta(\eta) + Q_s\Theta(\eta) = 0 \tag{14}$$

$$\emptyset''(\eta)(g_0)^2 + ScG\emptyset'(\eta)(g_0)^2 - ScG'\emptyset(\eta)(g_0)^2 + \frac{Nt}{Nb}\Theta(\eta) - R_c Sc\emptyset(\eta) = 0 \tag{15}$$

Then, multiplying equations (13) by $\frac{1}{(g_0)^4}$, (14) and (15) by $\frac{1}{(g_0)^2}$, we obtain equations (16) – (18).

$$G'''(\eta) + G(\eta)G''(\eta) - \varpi HG'(\eta) + J_t\emptyset(\eta)\varpi^2 = 0 \tag{16}$$

$$(1 + \frac{4S}{3})\Theta''(\eta) + PrG(\eta)\Theta'(\eta) + Nb\Theta(\eta)\emptyset(\eta)\varpi + Nt\Theta(\eta)\varpi + Q_s\Theta(\eta)\varpi = 0 \tag{17}$$

$$\emptyset''(\eta) + ScG\emptyset'(\eta) - ScG'(\eta)\emptyset(\eta) + \frac{Nt}{Nb}\Theta(\eta)\varpi - R_c Sc\emptyset(\eta)\varpi = 0 \tag{18}$$

However, due to large suction i.e. $\varpi \ll 1$, the series approximation solution is defined as:

$$\begin{aligned} G &= 1 + \varpi G_1 + \varpi^2 G_2 + \cdots \\ \Theta &= \Theta_0 + \varpi\Theta_1 + \cdots \\ \emptyset &= \emptyset_0 + \varpi\emptyset_1 + \cdots \end{aligned} \tag{19}$$

Taking the first, second and third derivatives of equation (19) with respect to η produces

$$\begin{aligned} G'(\eta) &= \varpi G_1' + \varpi^2 G_2' + \cdots \\ G''(\eta) &= \varpi G_1'' + \varpi^2 G_2'' + \cdots \\ G'''(\eta) &= \varpi G_1''' + \varpi^2 G_2''' + \cdots \\ \Theta' &= \Theta_0' + \varpi\Theta_1' + \cdots \\ \Theta'' &= \Theta_0'' + \varpi\Theta_1'' + \cdots \\ \emptyset' &= \emptyset_0' + \varpi\emptyset_1' + \cdots \\ \emptyset'' &= \emptyset_0'' + \varpi\emptyset_1'' + \cdots \end{aligned} \tag{20}$$

By putting equations (19) and (20) into equations (16) – (18), we simplify and equate corresponding powers of ϖ to have the following:

$$(1+\tfrac{4}{3}S)\theta_0''(\eta)+Pr\theta_0'(\eta)=0;\quad \theta_0(0)=1,\ \theta_0(\infty)=0 \tag{21}$$

$$\emptyset_0''(\eta)+Sc\emptyset_0'(\eta)=0;\qquad \emptyset_0(0)=1,\quad \emptyset_0(\infty)=0 \tag{22}$$

$$G_1'''(\eta)+G_1''(\eta)=0;\quad G_1(0)=0,\ G_1'(0)=1,\quad G_1'(\infty)=0 \tag{23}$$

$$(1+\tfrac{4}{3}S)\theta_1''(\eta)+Pr\theta_1'(\eta)+PrG_1(\eta)\theta_0'(\eta)+Nb\theta_0(\eta)\emptyset_0(\eta)+Nt\theta_0(\eta)+Q_s\theta_0(\eta)=0$$
$$\theta_1(0)=0,\theta_1(\infty)=0 \tag{24}$$

$$\emptyset_1''(\eta)+Sc\emptyset_1'(\eta)+ScG_1(\eta)\emptyset_0'(\eta)-ScG_1'(\eta)\emptyset_0(\eta)+\frac{Nt}{Nb}\theta_0(\eta)-R_cSc\emptyset_0(\eta)=0$$
$$\emptyset_1(0)=0,\quad \emptyset_1(\infty)=0 \tag{25}$$

$$G_2'''(\eta)+G_2''(\eta)+G_1(\eta)G_1''(\eta)-HG_1'(\eta)+J_t\theta_0(\eta)=0\ G_2(0)=0,\quad G_2'(0)=0,\quad G_2'(\infty)=0 \tag{26}$$

However, equations (21) – (26) have been solved numerically and the results have been obtained.

After solving equations (21) – (26) analytically, the following solutions for velocity $f'(\eta)$, heat $\theta(\eta)$ and nanoparticle concentration $\emptyset(\eta)$ are obtained:

$$f'(\eta)=e^{-\eta}+\varpi\left(\frac{-1}{2}e^{-2\eta}-H\eta e^{-\eta}-\frac{J_t}{M-1}e^{-M\eta}+\frac{1}{2}e^{-\eta}+\frac{J_t}{M-1}e^{-\eta}\right) \tag{27}$$

$$\theta(\eta)=e^{-M\eta}+\varpi\left(-M\eta e^{-M\eta}-\frac{M^2}{M+1}e^{-(1+M)\eta}-\frac{3Nb}{Sc(+4S)(M+Sc)}e^{-(Sc+M)\eta}+\frac{3Nt}{M(3+4S)}\eta e^{-M\eta}+\right.$$
$$\left.\frac{3Q_s}{M(3+4S)}\eta e^{-M\eta}+\frac{M^2}{M+1}e^{-M\eta}+\frac{3Nb}{Sc(+4S)(M+Sc)}e^{-M\eta}\right) \tag{28}$$

$$\emptyset(\eta)=e^{-Sc\eta}+\varpi\left(-Sc\eta e^{-Sc\eta}-\frac{(Sc)^2}{1+Sc}e^{-(1+Sc)\eta}+\frac{Sc}{1+Sc}e^{-(1+Sc)\eta}-\frac{Nt}{MNb(M-Sc)}e^{-M\eta}-R_c\eta e^{-Sc\eta}+\right.$$
$$\left.\frac{(Sc)^2}{1+Sc}e^{-Sc\eta}-\frac{Sc}{1+Sc}e^{-Sc\eta}+\frac{Nt}{MNb(M-Sc)}e^{-Sc\eta}\right) \tag{29}$$

where

$$\varpi=0.1, M=\frac{3Pr}{3+4S}. \tag{30}$$

3. Results and Discussion

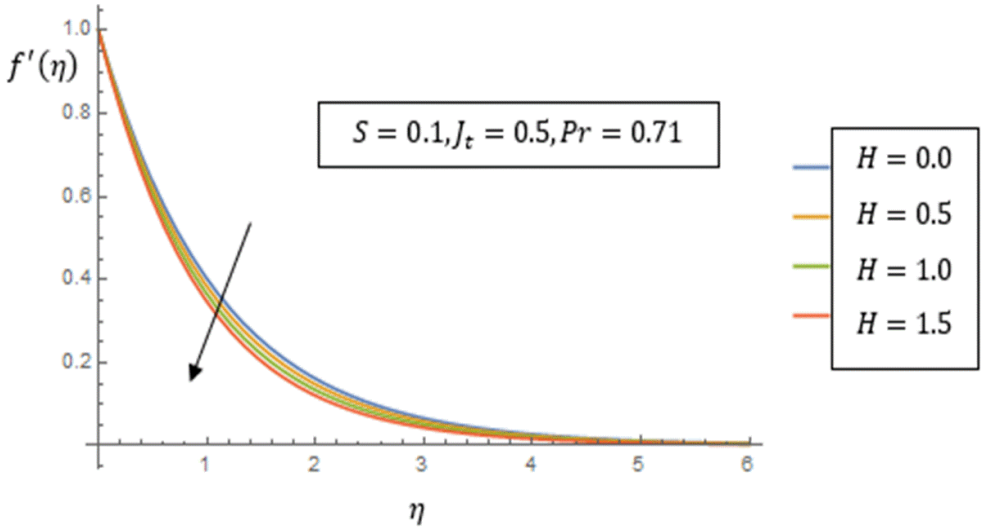

Fig 2. Influence of Hartmann factor on velocity

The effect of the Hartmann parameter on velocity is shown in Figure 2. Meanwhile, increase in its values leads to a decrease in the velocity. This is as a result of the fact that an opposing force drags the rate of the fluid flow backward thereby retarding the velocity. Thus, the Lorentz force is responsible for this phenomenon. Figure 3 illustrates the impact of the modified thermal Grashof number J_t on the fluid velocity near the stretching plate. This number J_t involves the influence of buoyancy force to viscous force and its enhancement entails an increasing trend in velocity distribution which breeds cooling at the surface of the plate.

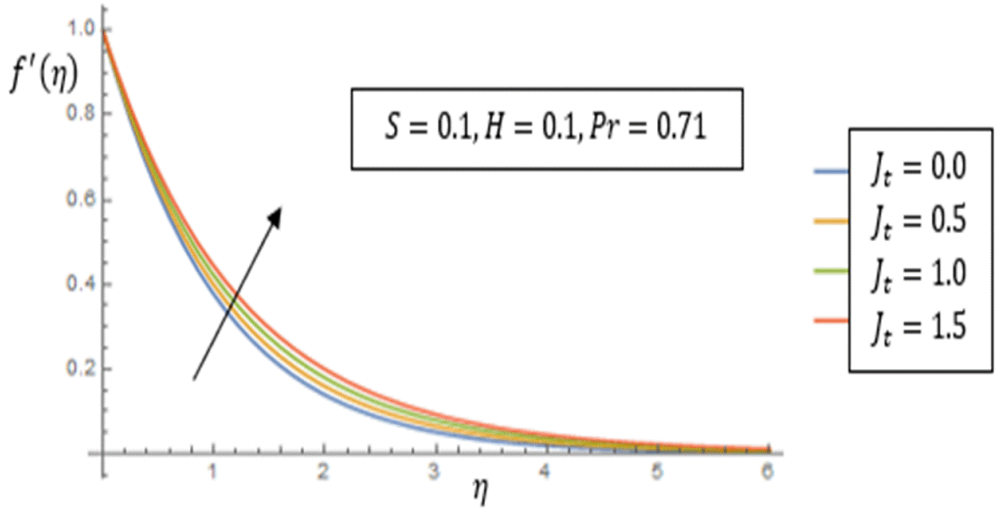

Fig. 3. Influence of Grashof number on velocity

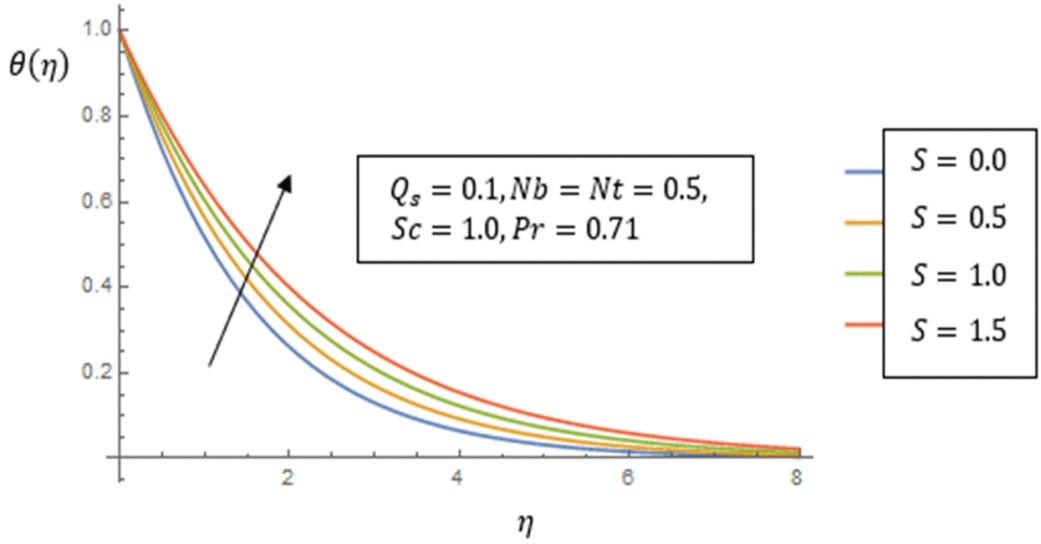

Fig. 4. Influence of radiation parameter on temperature

The evolution of radiation parameter S on temperature and concentration is displayed in Figures 4 and 5. Appreciating values of S causes an improvement of thermal boundary layers. This is due to the fact that the surface of the plate which is already heated releases more energy in form of heat. Thus, this leads to the augmentation of the temperature. Similarly, radiation transfers energy to the molecules immersed in a solution, leading to the generation of free radicals. These free radicals react with the dissolved metal ions to lessen them to their metallic status, resulting in the formation of nanoparticles and leading to an increase in their concentration.

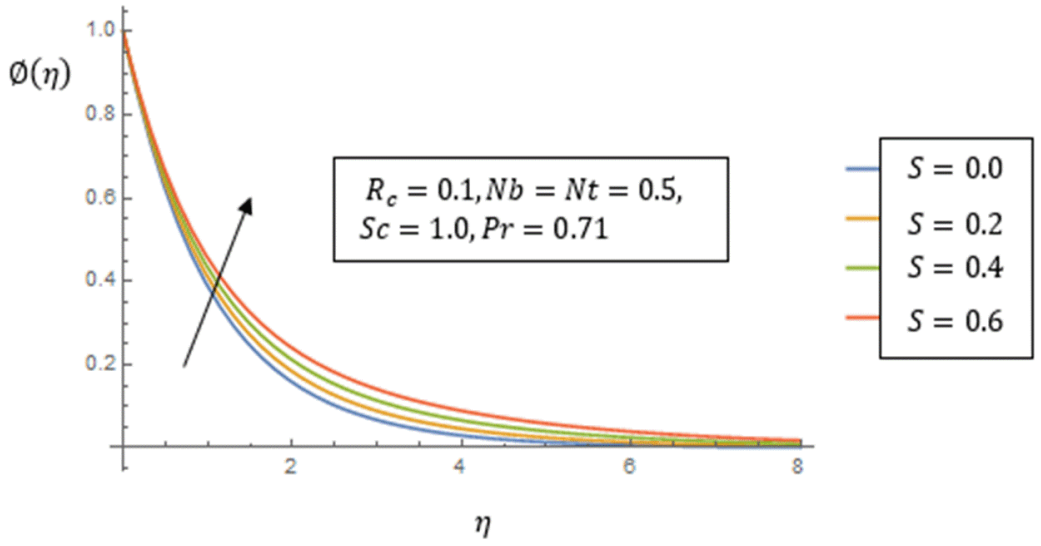

Fig. 5. Influence of radiation parameter on concentration

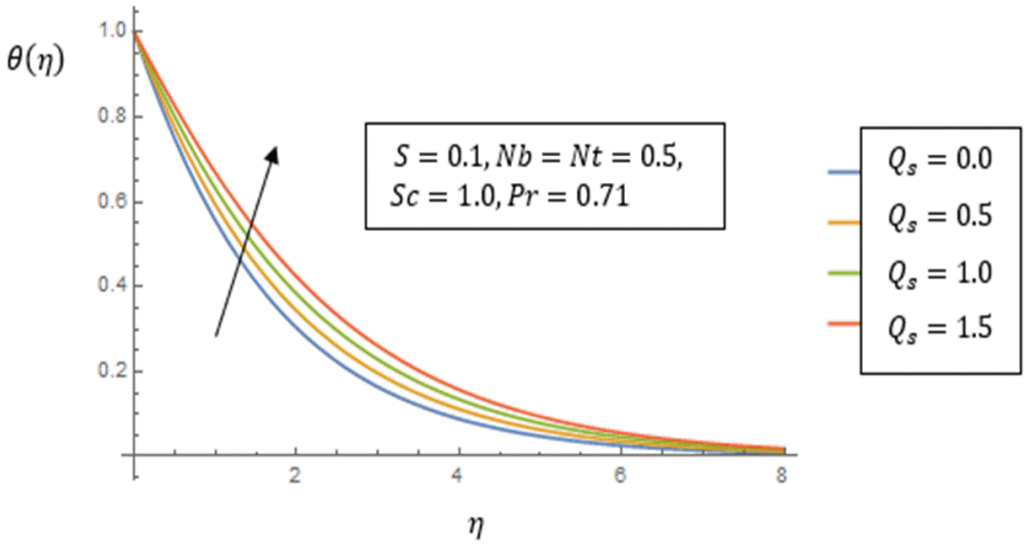

Fig 6. Influence of heat parameter on temperature

Figure 6 is indicative of the impact of heat source $(Q_s > 0)$ parameter on temperature. Heat is a type of energy which passes from a hotter body to a cooler one. Physically, the influx of heat $(Q_s > 0)$ to a system makes the kinetic energy of its molecules to increase, causing them to move quicker and hit with each other more frequently. As a result of this, the average kinetic energy of the particles increases and thus leads to a rise in temperature. The effect of Prandtl number Pr is depicted in **Figure 7**. As a dimensionless number which is expressed as the ratio of momentum diffusivity to thermal diffusivity of a fluid, it aids in the rate of cooling in conducting fluids. However, a surge in the Prandtl number implies that the fluid has higher momentum diffusivity relative to its thermal diffusivity. Thus, the fluid is more effective at transferring momentum, i.e. velocity, than it is at transporting heat, thereby resulting in a lower thermal transmission coefficient and smaller amount of heat removed from the surface. Therefore, heightening the Prandtl number leads to a fall in the thermal boundary layer which causes a decline in temperature of the fluid.

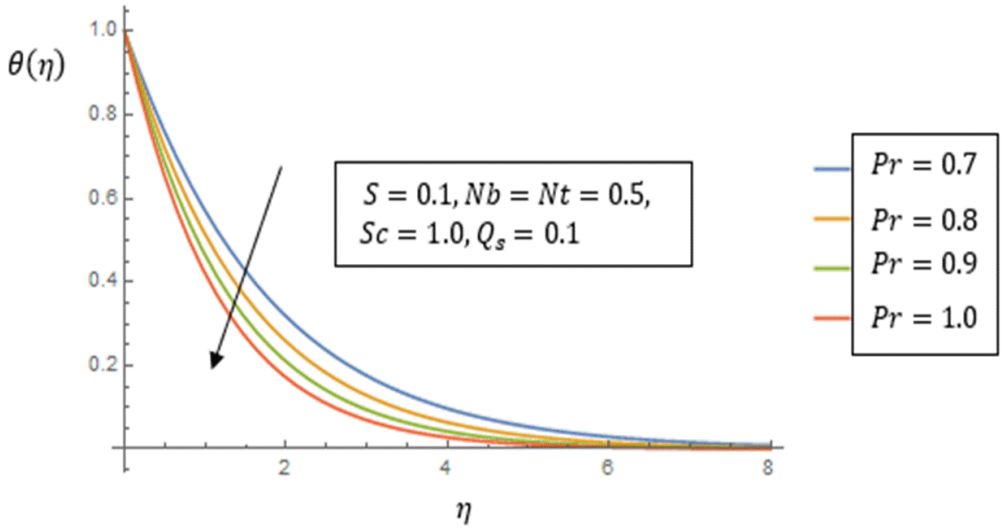

Fig 7. Influence of Prandtl factor on temperature

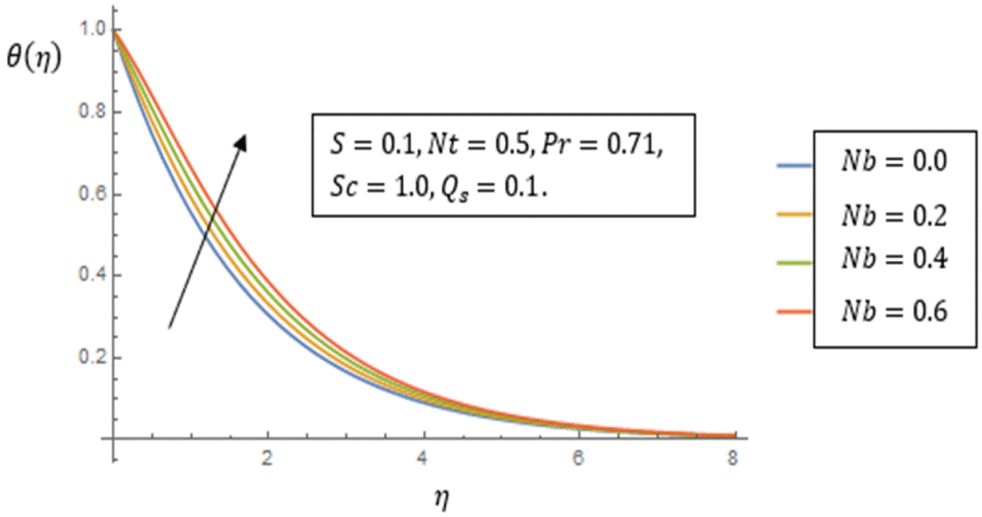

Fig 8. Influence of Brownian motion parameter on temperature

The impartation of Brownian motion, Nb, on temperature and nanoparticle concentration is shown in **Figures 8** and **9,** respectively. As the temperature of a fluid increases, the kinetic energy of its particles also rises, making them to travel faster and collide more often. Thus, this phenomenon between the particles brings about a growth in Brownian motion with an indirect impact of temperature increment. Conversely, an upsurge in this motion begets a decline in nanoparticle concentration. This is because Brownian motion causes nanoparticles to migrate haphazardly, striking each other in the fluid. As its value rises, the probability of nanoparticle hitting each other and accumulating also increases, thus breeding a decrease in the number of individual nanoparticles and an increase in the number of larger masses.

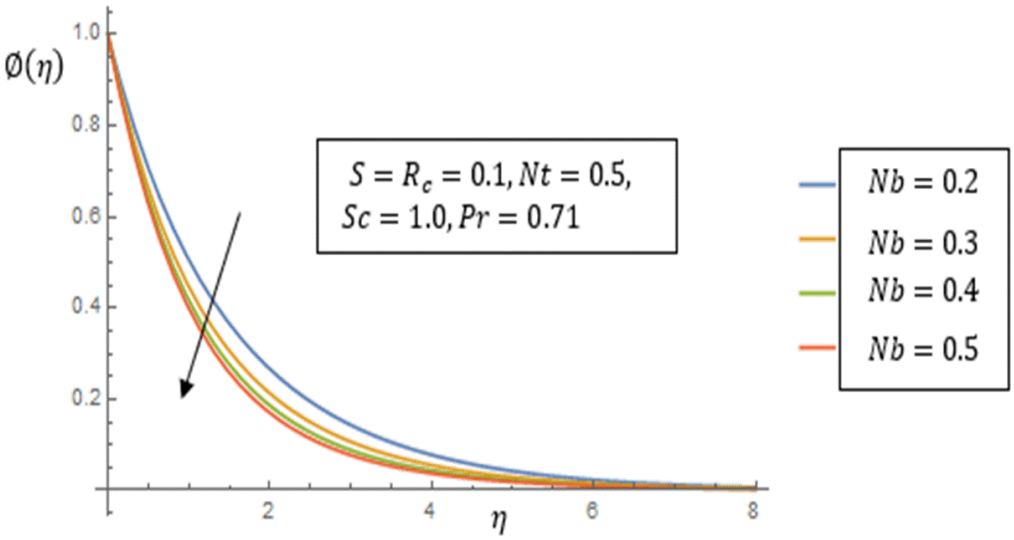

Fig 9. Influence of Brownian motion parameter on concentration

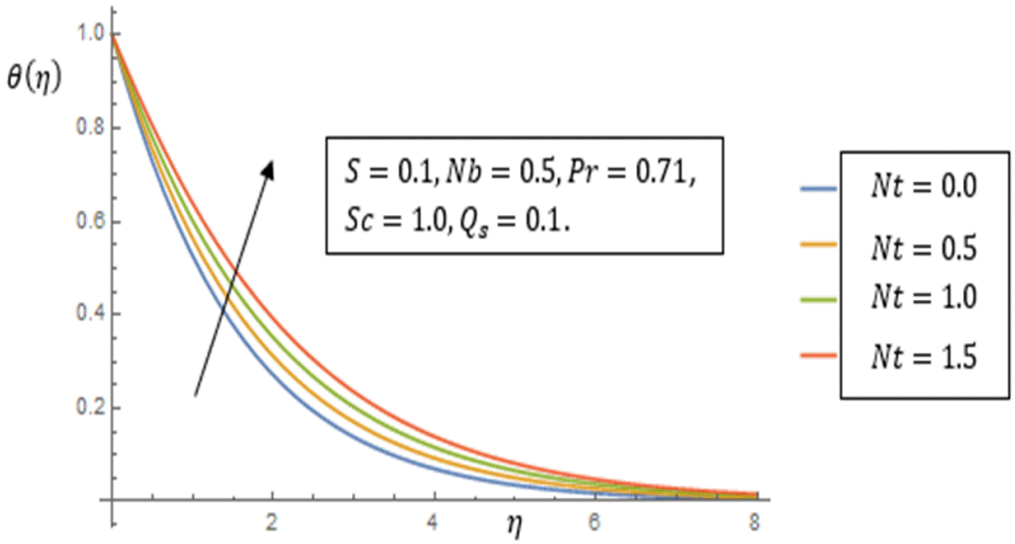

Figure. 10. Influence of thermomigration number on temperature

The impact of the thermo-migration parameter Nt on temperature and concentration is shown in **Figures 10** and **11**. Thermo-migration is the movement of particles in a fluid owing to temperature differences. When there is a change of temperature in a fluid with nanoparticles, such particles will possess a force that moves them toward areas of higher temperature. Hence, an augmentation in the value of this parameter produces the thickening of the thermal and mass boundary layers, which leads to a rise in the temperature and concentration.

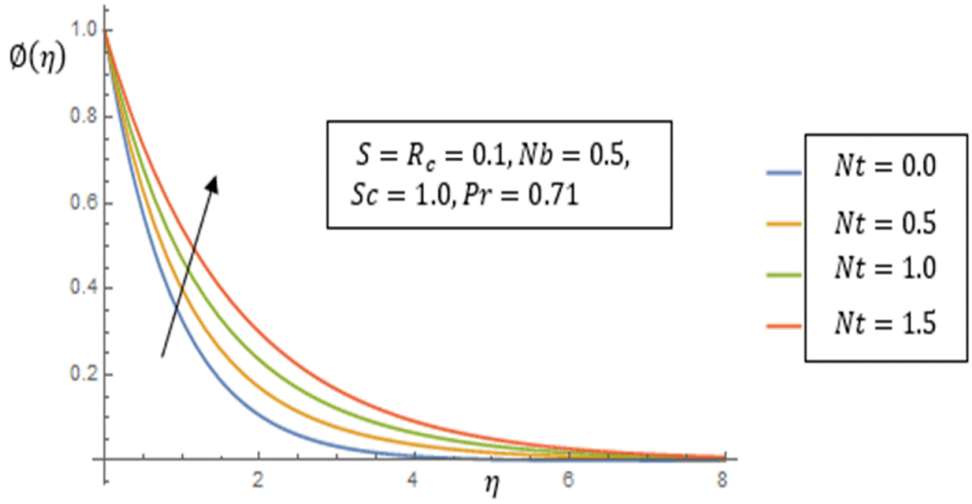

Figure. 11. Influence of thermomigration number on concentration

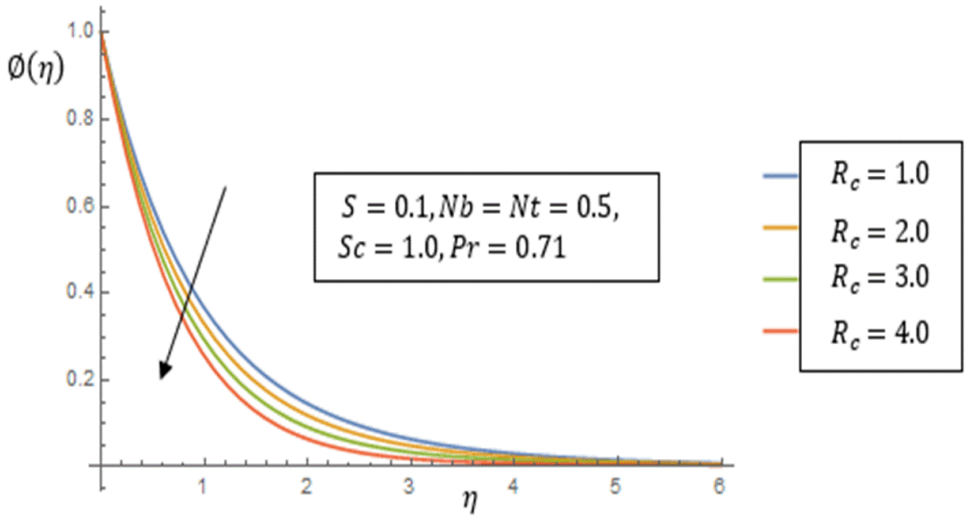

Figure. 12. Influence of chemical reaction parameter on concentration

The influence of chemical reaction R_c on concentration is depicted in **Figure 12.** However, a growth in temperature can quicken the reaction rate, which implies that the lessening of metal ions to nanoparticles happens quicker. Meanwhile, with a faster reaction, the nanoparticles may not possess sufficient time to develop to their required mass and may turn out to be unstable, thus leading to a reduction in concentration. **Figure 13** portrays the effect of Schmidt factor Sc on concentration. Due to the weaker nature of molecular diffusivity of the nano-particles caused by increasing values of the number, the diffusion rate reduces, hence there occurs a decrease in concentration.

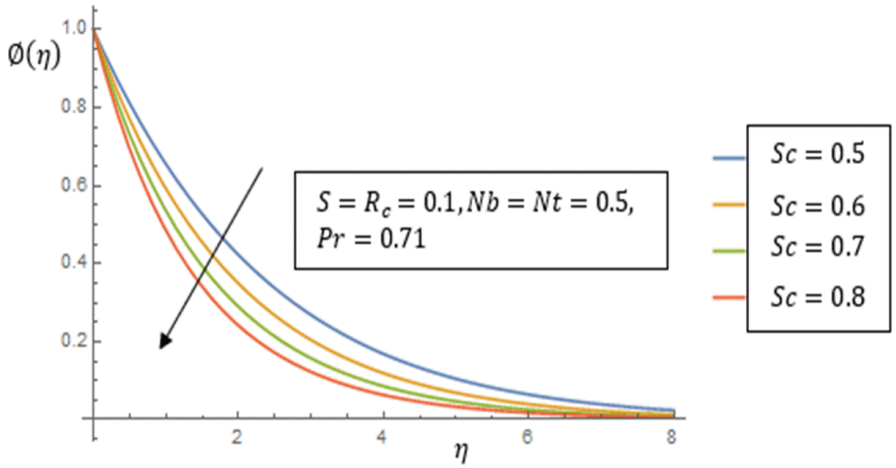

Figure. 13. Influence of Schmidt factor on concentration

Conclusion

The analysis of MHD nanofluid stream in the presence of enriched heat generation/absorption and thermo-migration have been examined. Thus, the conclusions regarding the scientific significance of the current study are stated below:

1. Improvement in the Hartman number H begets a fall in the fluid velocity while an increase in the local thermal Grashof number leads to the enhancement of rate of fluid flow.
2. Increasing the thermomigration parameters Nt causes a thicker, thinner thermal and mass boundary layer thickness with a corresponding rise in the temperature and concentration distribution.

3. As the heat Q_s, Brownian motion Nb and radiation S parameters surge, the thermal wall layer thickens followed by an upsurge in the temperature. Similarly, an increase in the radiation S parameter produces an enhancement in the concentration.
4. It is also observed that the concentration is decreased with rising chemical reaction R_c parameter.
5. **Improved understanding of MHD nanofluidic flow:** The research paper explores the flow behavior of a magnetohydrodynamic (MHD) nanofluid over a nonlinear exponentially stretched plate. This study contributes to the understanding of the behavior of nanofluids in the presence of a magnetic field and their reactivity to thermal source/sink and thermo-migration influences.
6. **Applications in energy engineering:** The results of this study can be applied in energy engineering, especially in the designing and optimization of MHD nanofluidic systems for heat transfer applications. Thus, the findings could aid to advance the proficiency of heat exchangers, boilers, and other energy systems that use nanofluids.
7. **Implications for materials science:** This study has significant implications for materials science since the application of nanoparticles into fluids can lead to improved thermal properties, making them useful for usage in heat transfer, energy storage, etc.
8. **Potential for biomedical applications:** The enriched thermal properties of nanofluids can also have implications for biomedical applications, such as hyperthermia treatments for cancer. The findings of this research paper could help in developing new and more effective hyperthermia treatment methods.
9. **Contribution to the development of numerical methods:** The numerical scheme used in this research paper can be applied to other fields of study such as computational fluid dynamics (CFD), and can aid the advancement of more accurate and efficient numerical methods for modelling fluid flow.

Acknowledgement

The authors sincerely appreciate Prof. Emeka Amos for his useful suggestions.

Author Contribution

Planning the method that will be suitable for achieving results by Uchenna Awucha Uka 1; Designing, supervision and responsibility for the organization, writing an original frame work and course of study by Uchenna Awucha Uka 1, Digbo Idika Iku 2, Great Edwin Esekhaigbe 3; Taking responsibility for the rationale and presentation of the findings by Uchenna Awucha Uka 1, Digbo Idika Iku 2, Great Edwin Esekhaigbe 3; Taking responsibility of the analysis by Uchenna Awucha Uka 1, Digbo Idika Iku 2, Great Edwin Esekhaigbe 3; Re-checking of the article before submission, not only on for spelling and grammar but also for intellectual content by Uchenna Awucha Uka 1, Digbo Idika Iku 2, Great Edwin Esekhaigbe 3; Critical review in planning the technique that will be appropriate for achieving noble results by Uchenna Awucha Uka 1, Digbo Idika Iku 2; Detailed analysis, proof-reading, review and editing of the manuscript by Uchenna Awucha Uka 1, Digbo Idika Iku 2, Great Edwin Esekhaigbe 3. All authors have read and given their full approval on the manuscript.

Conflict of Interest

The authors did not report any form of conflict of interest.

Research Funding

The current research did not receive any funding from any individual, institution or organization.

References

[1] Choudhary, S., Sharma, P. R., & Makinde, O. D. (2017). MHD slip flow and heat transfer over an exponentially stretching permeable sheet embedded in a porous medium with heat source. Frontiers in Heat and Mass Transfer (FHMT), 9(1).

[2] Mahdi, R. A., Mohammed, H. A., Munisamy, K. M., & Saeid, N. H. (2015). Review of convection heat transfer and fluid flow in porous media with nanofluid. Renewable and Sustainable Energy Reviews, 41, 715-734.

[3] Rashidi, M. M., Ganesh, N. V., Hakeem, A. A., & Ganga, B. (2014). Buoyancy effect on MHD flow of nanofluid over a stretching sheet in the presence of thermal radiation. Journal of Molecular liquids, 198, 234-238.

[4] Mustafa, M., Hayat, T., Pop, I., Asghar, S., & Obaidat, S. (2011). Stagnation-point flow of a nanofluid towards a stretching sheet. International Journal of Heat Mass Transfer, 54, 5588-5594.

[5] Vajravelu, K. (2001). Viscous flow over a nonlinearly stretching sheet. Applications in Mathematical Computations, 184, 864-873.

[6] Miklavcic, M., & Wang, C. Y. (2006). Viscous flow due to a shrinking sheet. *Quarterly Applied Mathematics*, 64, 283-290.

[7] Uka, U. A., Amos, E., & Nwaigwe, C. Chemical Reaction and Thermal Radiation Effects on Magnetohydrodynamic Nanofluid Flow Past an Exponentially Stretching Sheet.

[8] Devi, S. A., & Ganga, B. (2009). Effects of viscous and joules dissipation on MHD flow, heat and mass transfer past a stretching porous surface embedded in a porous medium. Nonlinear Analysis, Modelling and Control, 14(3), 303-314.

[9] Raju, C. S. K., Sandeep, N., Sugunamma, V., Babu, M. J., & Reddy, J. R. (2016). Heat and mass transfer in magnetohydrodynamic Casson fluid over an exponentially permeable stretching surface. Engineering Science and Technology, an International Journal, 19(1), 45-52.

[10] Mansour, M. A., El-Hakiem, M. A., & Kabeir, S. M. (2000). Heat and mass transfer in magnetohydrodynamic flow of micropolar fluid on a circular cylinder with uniform heat and mass flux. Journal of Magnetism and Magnetic Materials, 220, 259-270.

[11] Choi, S. U. S. & Eastman, J. A. (1995). Enhancing thermal conductivity of fluids with Nanoparticles. (No. ANL/MSD/CP-84938; CONF-951135-29). Argonne National lab.IL (United States).

[12] Buongiorno, J. (2006). Convective transport in nanofluids. Journal of Heat Transfer, 128(3), 240-250.

[13] Kuznetsov, A. V., & Nield, D. A. (2010). Natural convective boundary-layer flow of a nanofluid past a vertical plate. International Journal of Thermal Sciences, 49(2), 243-247.

[14] Sikiadis, B. C. (1961). Boundary-Layer behavior on continuous solid surfaces. AI Ch. EJ, 7, 26-28.

[15] Gaffar, S. A., Prasad, V. R., & Reddy, E. K. (2017). Mixed convection boundary layer flows of a non-Newtonian Jeffrey's fluid from a non-isothermal wedge. Ain Shams Engineering Journal, 8(2), 145-162.

[16] Tamayol, A., Hooman, K., & Bahrami, M. (2010). Thermal analysis of flow in a porous medium over a permeable stretching wall. Transportation in Porous media. 85(3), 661-676.

[17] Khani, F., Farmany, A., Raji, A. M., Aziz, A., & Samadi, F. (2009). Analytic solution for heat transfer of a third-grade viscoelastic fluid in non-Darcy porous media with thermophysical effects. Communications in Nonlinear Science and Numerical Simulation, 14(11), 3867-3878.

[18] Hayat, T., Awais, M., Safdar, A., & Hendi, A. A. (2012). Unsteady three dimensional flow of couple stress fluid over a stretching surface with chemical reaction. Nonlinear Analysis: Modelling and Control, 17(1), 47-59.

[19] Awucha, U. U., & Okechukwub, A. (2022). Soret Dissipation Effect On Heat And Mass Transmission Of Non-Newtonian Casson Radiative Nanofluid Flow With Lorentz Drag And Rosseland Radiation. Journal of Pure & Applied Sciences, 21(2), 120-127.

[20] Venkateswarlu, M., & Padma, P. (2015). Unsteady MHD convective heat and mass tranfer in a boundary layer flow past a vertical permeable plate with thermal radiation and chemical reaction. International Conference on Computational Heat and Mass Transfer-2015, Procedia Engineering, 127, 791-799.

[21] Pudhari, S. (2018). Hall current effect on the MHD flow of Newtonian fluid through a porous medium. International Journal of Applkied Engineering Research, 13(7), 4637-4651.

[22] Juliyanto, B., Widodo, B., & Imron, C. (2018, April). The effect of heat generation on mixed convection flow in nano fluids over a horizontal circular cylinder. In Journal of Physics: Conference Series (Vol. 1008, No. 1, p. 012001). IOP Publishing.

[23] Bestman, A. R. (1990). The boundary layer flow past a semi-infinite heated porous for two-component plasma. *Astrophysics and Space Science*, 173, 93-100.

Journal of Investigations on Engineering & Technology
Volume 6, Issue 1, 28-35, 2023

ISSN: 2687-3052

Research Article

A Comparison Study: Image Restoration Based on Two Heuristic Algorithms

Nurşah DİNCER[1], Kerim DİNCER[2], Emel ARSLAN[3]

(Received: 30.03.2023, Accepted: 05.07.2023, Published Online: 26.07.2023)

Keywords
Blurred Images
Heuristic Algorithms
Image Restoration
Artificial Bee Colony Algorithm
Firefly Algorithm

Abstract: In computer science, optimization can be defined as maximizing or minimizing the result. Heuristic algorithms have been developed inspired by nature and to solve different optimization problems. In this study, Artificial Bee Colony (ABC) Algorithm and Firefly Algorithm (FA) have been explained in detail and a comparison between these two algorithms has been implemented. The comparison between these two algorithms is made for image restoration by using a dataset. Image restoration is the process of reducing or eliminating data loss or deterioration that may occur during the creation of an image. The loss of efficiency in the image (reducing the visual appearance of the image) is caused by noise. It is the process of obtaining the original image from the distorted image, given the knowledge of distorting factors. There are many methods applied in the literature for image restoration. In this study, two of the evolutionary algorithms have been used for this purpose and analyzed. The data set used in the study was taken from the Kaggle website. The comparison metrics are PSNR (Peak Signal-to-Noise Ratio) and MSE (Mean Squared Error). This study shows that ABC Algorithm has better results than FA on the selected 20 images dataset used for blurred image restoration. According to the results obtained, it was seen that the ABC algorithm performed % 85 better than FA.

1. Introduction

Optimization can be defined as using the smallest amount of data optimally. The aim of optimization is maximization in some studies and minimization in some studies. For any problem, it is to obtain the best solution among all solutions under the given conditions. This concept has emerged, inspired by the behaviors of living things to survive in their daily lives. For example, the reaction of one of the individuals in the herd to the danger may turn into a joint action by affecting the other individuals. Inspired by creatures living in swarms, scientists developed swarm-based optimization algorithms. With these developed algorithms, real-world problems and computer problems can be solved. It has been seen that creative solutions can be obtained by adapting the survival behaviors of living things to problems [1, 2].

ABC algorithm and FA were used in this study. For image restoration, a comparison was made using a dataset of text photos (book titles and readings) with and without the motion blur effect from the Kaggle website. This dataset was used to analyze the performance difference between the ABC algorithm and FA in blurry image restoration. 20 randomly selected images from the data set were used.

[1] Karadeniz Technical University, Department of Computer Technologies, Trabzon, Türkiye
[2] Karadeniz Technical University, Department of Energy Systems Engineering, Trabzon, Türkiye
[3] Istanbul University-Cerrahpaşa, Department of Computer Engineering, İstanbul, Türkiye

Corresponding Author and e–mail address: Nurşah DİNCER nursahdincer@ktu.edu.tr

Some studies in the literature are shown in the literature review section in the form of a table. The data set and evaluation criteria used in the study are mentioned in the material and method section. In the section on algorithms, there is information about the ABC algorithm and FA. In the conclusion part, the findings obtained from the study are presented comparatively.

Literature Review

In this section, several studies with image restoration using the ABC algorithm and FA are introduced. These studies are from 2011 to 2023. The number, authors, purpose, used algorithms, and evaluation metrics of these studies are given in Table 1.

Table 1. The studies on image restoration using the ABC algorithm and FA

Number	Authors	Purpose	Used Algorithms	Evaluation Metrics
[3]	Kumar et al. (2022)	Using the histogram of low contrast images and depth images aimed to increase contrast and remove unwanted noise	FA	PSNR, RMSE, UQI, MAE and MSE
[4]	Banharnsakun (2022)	It is aimed to find the most suitable filter coefficient to remove image noise	ABC	-
[5]	Gao et al. (2023)	In this study, the aim is to develop a hybrid algorithm to optimize BPNN for image restoration	FA and Genetic Algorithm	PSNR and MSE
[6]	Sun et al. (2022)	Aimed to solve problems of poor image quality, loss of detail information, and excessive brightness gain during image enhancement in low-light environments	ABC	Standard Deviation, Average Gradient, Information Entropy
[7]	Yang et al. (2016)	By using ABC algorithm, suggests a new technique for image restoration	ABC	PSNR
[8]	Li & Chan (2011)	A complex-fuzzy approach is used and complex fuzzy sets is proposed to deal with the problem of adaptive image noise cancelling	ABC	PSNR
[9]	Kockanat et al. (2012)	To design 2D FIR digital filters for the noise elimination on the noisy images, the ABC algorithm has been applied	ABC	Mean Value, Standard Deviation and PSNR
[10]	Sánchez-Ferreira et al. (2019)	To forecast the model parameters by using bio-inspired optimization, a restoration algorithm is proposed	ABC and Differential Evolution (DE)	NR-IQA
[11]	Kumar et al. (2020)	Proposes an object restoration approach in which images are affected by the salt & pepper noise modified by a median filter based on fuzzy logic	Modified Firefly Optimization Algorithm (MFOA) and Richardson-Lucy Algorithm	SDME and PSNR
[12]	Savithri & Kousalya (2016)	Aim of the paper is to carry out Bandelet transform with FA on SAR images	FA and Bandlet Transform with Firefly Algorithm (BFA)	MSE, ENL, SSI, SMPI, ESI and PSNR
[13]	Csam et al. (2017)	Offers the distinctive hybrid methods which evacuate the mixed type of noise from the images	FA	Root Mean Squared Error (RMSE) and PSNR
[14]	Sam et al. (2019)	Uses a blend of filters to determine the noise from the images	FA	RMSE, PSNR and SSIM

Looking at the studies in the literature, it is seen that the ABC algorithm and FA are used. However, no performance comparison has been made by using these two algorithms together in any study. So, it is not known which algorithm is more performant for image restoration. For this reason, in this study, it was investigated which one was more effective for image restoration using the ABC algorithm and FA.

3. Material and Method

Swarm intelligence is decentralized control, the collective behavior of natural or artificial self-organizing systems. Especially, it is focused on the collective behavior and environments of animals or beings. Animals do not have any control mechanism by themselves but, interestingly, they can find foods easily, feel environmental attacks, and they can respond to foes. They have simple communication and this time they spend less cost they create a flexible and robust swarm structure and they act intelligently to solve their problems when they encounter any problems. Some scientists and engineers are interested in interesting techniques of animals because in many areas these kinds of swarm intelligence algorithms are used to resolve difficult problems [15].

All of the experimental work was implemented in MATLAB® R2015a and performed on an Intel(R) Core™ i7-10870H CPU @ 4.80 GHz, 32 GB RAM and an x64 based processor.

3.1. Data set

In this study, the dataset which is photos of text (book titles and readings) with and without the motion blur effect is selected from Kaggle to present the performance differences between ABC Algorithm and FA. This dataset provides motion blur-affected and unaffected images. This dataset includes 184 images of various book titles and texts both motion-blurred and normal. For this study, 20 blurred images are selected from these 184 images [16].

3.2. Image quality

In digital imaging, the image is captured by the camera and converted into digital signals. This image may not be the same as the original image, subject to various distortions when shown to the user. These distortions are caused by different factors such as Gaussian noise, compression, and transmission disturbances. Control of the image quality is important for the digital imaging system to evaluate the image quality optimally.

The image can be checked with metrics of image quality. Quality of image metrics can be used to compare algorithms such as compression, restoration, and restoration techniques in images. Full reference quality metrics can be used to directly compare the target image and the reference image [17].

In this study, MSE and PSNR are used to make a comparison between ABC Algorithm and FA by using the blurred image dataset.

3.2.1 Mean squared error (MSE)

The MSE measures the average square difference between real and ideal pixel values. The calculation of this metric is basic but it does not correspond to human quality perception. The smaller the mean square error, the closer it is to the original. It can be calculated by using Eq. 1 [18].

$$MSE = \frac{1}{n}\sum_{i=1}^{n}(Y_i - \hat{Y}_i)^2 \tag{1}$$

Where Y_i is the actual values, $\hat{Y}_i$ is the predicted values, and n is the number of data.

3.2.2 Peak signal to noise ratio (PSNR)

PSNR is a metric that indicates the rate of the maximum possible power of a signal to the power of noise on the signal. The signal represents the original data and the noise represents the compression-related error. When comparing compression codes, PSNR can be considered an approach to human quality perception. PSNR value can be calculated by using Eq. 2 [19].

$$PSNR = 10.log_{10}\left(\frac{MAX_i^2}{MSE}\right) \tag{2}$$

Where, MAX_i is the maximum possible pixel value of the image. MSE is mean squared error.

3.2.3. Image restoration

Image restoration is a basic method of obtaining the original state of a blurred image. To be able to find the optimal solution $u \in R^m$ based on the following model:

$$f = Au + \varepsilon \tag{3}$$

where $A \in R^{m \times m}$ is a blurring operator, $\varepsilon \in R^m$ is an unknown Gaussian white noise with variance σ^2, f and u denote the indicate degraded image and the original image, respectively [20].

4. Algorithms

Detailed information about the ABC algorithm and FA are included in this section under subsections.

4.1. Artificial Bee Colony (ABC) Algorithm

ABC algorithm is the algorithm developed by the modeling foraging attitude of bees. In a natural bee colony, there is task sharing between bees according to the work to be done and bees do this work by themselves without a central unit. Job sharing and self-organization are the two important features of swarm intelligence. Bees go to food sources to find honey, pollen, or nectar. The factors such as proximity of the food resource to the nest, type, density of nectar, and facilitate of extracting the nectar determine the value of the food source. Addressing a single factor rather than simultaneously evaluating many such factors may simplify the situation in problem-solving. It is the responsibility of the worker bee to bring the nectar from the previously discovered sources to the hive. They also share information about the quality and location of the resource they visit with other bees in the hive. Non-tasked worker bees are looking for new food sources where nectar can be collected. There are two types of bee groups that are ambiguous; the first one is explorer bees, who seek indiscriminate resources with the help of instinct or external factors. The second one is the lookout bee group. These are bees waiting in the hive and watching the bees in charge and using the information shared by these bees, they turn to a new source. Information sharing is an important factor among bees. The location and quality of the food source are shared with other bees thanks to the dancing ability of the bees. The bee, who is familiar with the food source, starts to dance, and the other bees touch it and get information about the food source. ABC algorithm tries to find the place of the food resource with the most nectar and tries to find the solution that gives the minimum or maximum of the problem in space solutions [21].

Algorithm 1. Pseudocode of ABC Algorithm [22]

1. By using x_i, initialize the population of solutions
2. Appraise the population
3. period=1
4. Repetition
5. For the working bees by evaluating solutions, Generate new solutions v_i.
6. Implement the greedy choosing process between x_i and v_i
7. If the fitness value of v_i is worse than x_i $failure_i$=$failure_{i+1}$, if the solution is improved $failure_i$=0
8. For the solutions x_i compute the probability values P_i
9. Generate the new solutions v_i for the onlookers from the solutions x_i chosen depending on P_i and appreciate them.
10. Between x_i and v_i, implement the greedy choosing process
11. Define the abandoned solution for the rover bee, if it exists, and modify it with a new randomly produced solution x_i
12. Memorize the best solution reached so far
13. period=period+1
14. Until period=maximum period number of $failure_i$ =limit

4.2. Firefly Algorithm (FA)

Fireflies are small winged insects that can produce cold and flashing lights to attract other insects of their kind. Female fireflies try to attract men by mimicking the light signals of different species. Their energies emerge in the form of light and repeat in a cyclic manner [23]. The FA is one of the optimizing swarm intelligence approaches developed by Yang. It is inspired by the attenuation of light relative to distance and the attractiveness of insects. Three assumptions are adopted in the FA.

1. All fireflies are considered sexless. So all fireflies can affect the rest of the other fireflies.

2. The firefly with less light moves towards the firefly with bright light. The brightness changes depending on the distance. If the brightness level is equal, random motion occurs.

3. The fitness function determines the brightness. According to the result of this function, the best one is the brightest [24].

N firefly flock is used in the FA. C_i refers to the solution of the ith firefly. $f(C_i)$ indicates the cost of the solution, ie the distance to the best. For all fireflies, C_i has as many elements as the problem size and is initialized with random values. Each candidate solution to be optimized represents the glow/light intensity (I) of the firefly (Eq. 4).

$$I = I_0 e^{-\gamma r} \tag{4}$$

I_0: Starting light density
γ: Light absorption coefficient
r: Distance between two fireflies

Algorithm 2. Pseudocode of Firefly Algorithm [25]

Objective function $f(c)$, $c = (c_1, \ldots, c_d)^T$
Create an initial population of fireflies c_i (i=1, 2, …, n)
Light density I_i *at* c_i *is decided by* $f(c_i)$
Define light absorption coefficient γ
while (t<$MaxGeneration$)
  for i=1:n *all n fireflies*
    for j=1:n *all n fireflies*
      if (I_j> I_i), *Move firefly i towards j in d-dimensions;*
      end if Attractiveness varies with distance r via exp [$-\gamma r$]
    Appraise new solutions and update light density
    end for j
  end for i
Sort the fireflies and find the current best
end while
Postprocess results and visualization

The attraction of the firefly depends on its brightness and distance (Eq. 5)

$$\beta = \beta_0 e^{-\gamma r^2} \tag{5}$$

β: Firefly attractiveness.
β_0: The attraction value when r is 0, indicating the distance between two fireflies (It can take values between 0 and 1).

Depending on the value in β expression, the *i*th firefly, which is less attractive, moves towards the *j*th firefly, which is more attractive than itself. This movement is determined by Eq. 6.

$$x_i^{t+1} = x_i + \beta_0 e^{-\gamma r_{ij}^2}\left(x_j - x_i\right) + \alpha \varepsilon_i^t \tag{6}$$

x_i: Applicant solution of *i*th firefly
x_j: Applicant solution of *j*th firefly
ε_i: It is determined by the Gaussian distribution

The distance between the two fireflies is examined by the Cartesian distance formula (Eq. 7) [26].

$$r_{ij} = \left|x_i - x_j\right|^2 = \sqrt{\sum_{k=1}^{d}(x_{i,k} - x_{j,k})^2} \tag{7}$$

5. Results

PSNR and MSE values were used to compare the performance of the ABC Algorithm and FA in image restoration. A high PSNR value indicates high image quality and low noise level. There is an inversely proportional relationship between PSNR and MSE. Therefore, a lower MSE value means fewer errors and higher image quality [18, 19].

The dataset consists of 20 images. As an example, some of these images are shown in Figure 1, Figure 2, and Figure 3. Here, a) shows the original image, b) shows a state after the ABC algorithm application, and c) shows a state after the FA application.

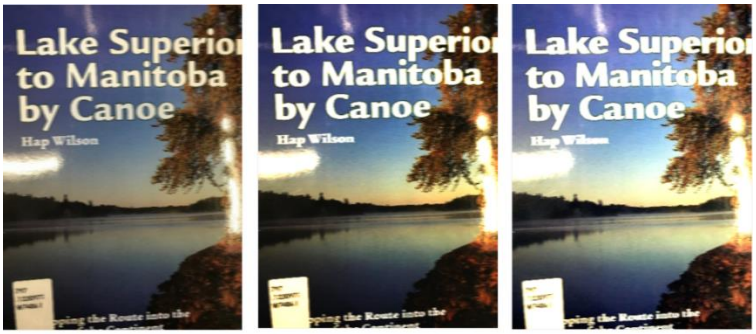

(a) (b) (c)

Figure 1. a) Original image b) After applying ABC algorithm c) After applying FA

(a) (b) (c)

Figure 2. a) Original image b) After applying ABC algorithm c) After applying FA

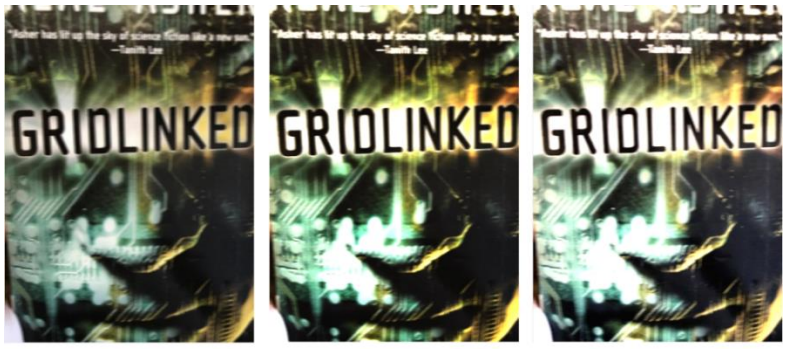

(a) (b) (c)

Figure 3. a) Original image b) After applying ABC algorithm c) After applying FA

PSNR and MSE values of the images are given in Table 1. It is desired to obtain images with high PSNR value and low MSE value. According to Table 1, when PSNR and MSE values of the first 17 images are examined, it is seen that ABC algorithm gives better results than FA. In 17 of the 20 images, the ABC algorithm prevailed over FA. In other words, it is 85% more successful in comparison with FA. In addition, the arithmetic mean of PSNR and MSE values obtained by these two algorithms for 20 images is given in the last column of Table 1. The average PSNR of the ABC algorithm is 27.74, while that of the FA is 26.14. In other words, the PSNR value of the ABC algorithm is higher. The average MSE of the ABC algorithm is 114.89. The average MSE of the FA is 162.07. On the other hand,

the MSE value of the ABC algorithm is lower. As a result, it was seen that it would better result to use the ABC algorithm instead of FA in image restoration studies.

Table 1. PSNR and MSE values of images with ABC algorithm and FA

Original Image	PSNR		MSE	
	Value of PSNR (ABC)	Value of PSNR (FA)	Value of MSE (ABC)	Value of MSE (FA)
Image 1	28.16	26.77	99.10	136.67
Image 2	26.30	25.80	152.29	170.99
Image 3	28.92	24.74	83.24	218.23
Image 4	27.37	25.97	118.88	164.26
Image 5	27.50	25.48	115.45	183.99
Image 6	29.56	25.84	71.88	169.26
Image 7	30.52	25.90	57.62	166.87
Image 8	25.99	25.34	163.40	189.75
Image 9	27.97	24.88	103.54	211.21
Image 10	30.02	27.26	64.57	122.08
Image 11	29.07	24.92	80.47	209.18
Image 12	27.02	26.06	129.03	160.83
Image 13	29.53	25.27	72.38	193.21
Image 14	26.00	25.43	163.30	185.95
Image 15	27.76	27.47	108.79	116.42
Image 16	25.78	25.61	171.51	178.29
Image 17	27.61	27.51	112.59	115.20
Image 18	26.19	26.64	156.06	140.92
Image 19	27.12	27.34	125.94	119.73
Image 20	26.42	28.66	147.95	88.49
Arithmetic Mean	27.74	26.14	114.89	162.07

6. Conclusions

This study, it is aimed to compare the performances of the ABC algorithm and FA for image restoration. First of all, a summary of the existing studies in the literature is given. Then, information about the ABC algorithm and FA used in the study is given. The experimental study is shown in the conclusion section. The performance of the algorithms was compared according to PSNR and MSE values. A dataset (book titles and readings) from Kaggle's text photos with and without the motion blur effect was used. 20 random images with motion blur effects were taken from this dataset. The application was made in MATLAB R2015a. As a result of the study, it was seen that the ABC algorithm performed better than FA. The ABC algorithm outperformed 17 of 20 images. This performance is also seen when the average PSNR and MSE values are examined. As a result, it is recommended to use the ABC algorithm in image restoration studies. The ABC algorithm had higher PSNR and lower MSE values on 17 of 20 images compared to FA. The average PSNR of the ABC algorithm for 20 images is 6.12% higher than that of FA. The average MSE value of the ABC algorithm is 29.11% lower than that of FA. As a result, the use of the ABC algorithm in image restoration studies gives better results than FA.

Conflict of Interest

The authors confirm that there is no known conflict of interest or common interest with any institution/organization or person.

References

[1] Bunday, B. D. (1985). Basic Linear Programming.

[2] Kahaner, D., Moler, C., & Nash, S. (1989). Numerical methods and software.

[3] Kumar, N., Kumar, A., & Kumar, K. (2022). Color Image Contrast Enhancement Using Modified Firefly Algorithm. *International Journal of Information Retrieval Research (IJIRR)*, 12(2), 1-18.

[4] Banharnsakun, A. (2022). Aerial Image Denoising Using a Best-So-Far ABC-based Adaptive Filter Method. *International Journal of Computational Intelligence and Applications*, 21(04), 2250024.

[5] Gao, Q., Gao, Y., Zhou, W., & Hua, T. (2023). Bpnn-Based Image Restoration Algorithm Optimized Using Hybrid Genetic Algorithm. *SSRN*.

[6] Sun, Y., Zhao, Z., Jiang, D., Tong, X., Tao, B., Jiang, G., ... & Fang, Z. (2022). Low-illumination image enhancement algorithm based on improved multi-scale Retinex and ABC algorithm optimization. *Frontiers in Bioengineering and Biotechnology.*

[7] Yang, J., Hu, D., & Yu, W. (2016). Artificial Bee Colony Algorithm for Image Restoration. In *2016 4th International Conference on Electrical & Electronics Engineering and Computer Science (ICEEECS 2016)*. Atlantis Press.

[8] Li, C., & Chan, F. (2011). Complex-Fuzzy Adaptive Image Restoration–An Artificial-Bee-Colony-Based Learning Approach. In *Intelligent Information and Database Systems: Third International Conference, ACIIDS*. Springer Berlin Heidelberg.

[9] Kockanat, S., Karaboga, N., & Koza, T. (2012). Image denoising with 2-D FIR filter by using artificial bee colony algorithm. In *2012 International Symposium on Innovations in Intelligent Systems and Applications*. IEEE.

[10] Sánchez-Ferreira, C., Coelho, L. S., Ayala, H. V., Farias, M. C., & Llanos, C. H. (2019). Bio-inspired optimization algorithms for real underwater image restoration. *Signal Processing: Image Communication*, 77, 49-65.

[11] Kumar, N., Dahiya, A. K., & Kumar, K. (2020). Image restoration using a fuzzy-based median filter and modified firefly optimization algorithm. *Int J Adv Sci Technol*, 29(4), 1471-1477.

[12] Savithri, K. M., & Kowsalya, G. (2016). SAR image despeckling using Bandlet transform with firefly allgorithm. *International Journal of Advanced Engineering Technology*.

[13] Csam, B. B., Tharika, F. G., Luxci, K. I., & Kumar, N. V. R. (2017). A survey on image restoration using hybrid channel based on firefly algorithm. *International Conference on Information Communication and Embedded Systems (ICICES)*. IEEE.

[14] Sam, B. B., & Fred, A. L. (2019). Denoising medical images using hybrid filter with firefly algorithm. *International Conference on Recent Advances in Energy-Efficient Computing and Communication (ICRAECC)*. IEEE.

[15] Bonabeau, E., Dorigo, M., Theraulaz, G., & Theraulaz, G. (1999). Swarm intelligence: from natural to artificial systems.

[16] https://www.kaggle.com/datasets (Date Accessed: 22.07.2022).

[17] Zhai, G., & Min, X. (2020). Perceptual image quality assessment: a survey. Science China Information Sciences, 63, 1-52.

[18] https://en.wikipedia.org/wiki/Mean_squared_error (Date Accessed: 25.07.2022).

[19] Hore, A., & Ziou, D. (2010). Image quality metrics: PSNR vs. SSIM. 20th international conference on pattern recognition. IEEE.

[20] Demoment, G. (1989). Image reconstruction and restoration: Overview of common estimation structures and problems. IEEE Transactions on Acoustics, Speech, and Signal Processing, 37(12), 2024-2036.

[21] Karaboğa, D. (2014). Yapay Zeka Optimizasyon Algoritmaları.

[22] Basti, M., & Sevkli, M. (2015). An artificial bee colony algorithm for the p-median facility location problem. *International Journal of Metaheuristics*, 4(1), 91-113.

[23] Dekhici, L., Redjem, R., Belkadi, K., & El Mhamedi, A. (2019). Discretization of the firefly algorithm for home care. *Canadian Journal of Electrical and Computer Engineering*, 42(1), 20-26.

[24] Aydilek, İ. B. (2017). Değiştirilmiş ateşböceği optimizasyon algoritması ile kural tabanlı çoklu sınıflama yapılması. *Gazi Üniversitesi Mühendislik Mimarlık Fakültesi Dergisi*, 32(4), 1097-1108.

[25] Karaarslan, E., & Zengin, K. (2016). Ateş böceği algoritması ile haftalık ders programı hazırlama. EEB 2016 Elektrik-Elektronik ve Bilgisayar Sempozyumu, 11-13.

[26] Yang, X. S. (2009). Firefly algorithms for multimodal optimization. *In Stochastic Algorithms: Foundations and Applications: 5th International Symposium*.

Journal of Investigations on Engineering & Technology
Volume 6, Issue 1, 36-44, 2023

ISSN: 2687-3052

Research Article

Comparative Study Between the Track Solar PV and Fixed Solar PV in Water Pumping System

Jamilu Ya'u MUHAMMAD[1*], Faru Faruk TUKUR [2], Ibrahim Umar IBRAHIM [3], Adamu Yusuf ABDULLAHI[4], Ibrahim Sule Ahmad ABDULMAJEED [5], Yusuf ALHAJI[6]

(Received: 15.11.2022, Accepted: 25.03.2023, Published Online: 26.07.2023)

Keywords
Efficiency
Electric Motor
Flow rate
Pump
Solar PV

Abstract: Solar pumping system is among the renewable energy techniques developed over the decades, and this system is used to solve the problem of water and food scarcity since the amount of rainfall is consistently decreasing especially in the northern part of Nigeria. This research tends to design the solar pumping system with automatic tracking of the solar PV to optimize the amount of solar irradiance extracted by the solar PV under the climatic conditions of Kano State, Nigeria, and it compares the results obtained with the system without tracking technique. It was found that the total average amounts of water pumped by the tracked and fixed systems were 1370 m^3/day and 804 m^3/day for sunny days. And for cloudy days they were 750 m^3/day and 714 m^3/day. It was recommended to develop an energy storage battery with very sensitive material to store the solar energy extracted to cover the gap between sunny and cloudy days.

1. Introduction

Food and water are among the necessities in the life of both animals and plants, but food scarcity is the major challenge of mankind in most developing countries like Nigeria. This food scarcity is due to the low rainfall rate especially in the Northern part of Nigeria and lack of the irrigation channels in the areas. Local farmers are suffering from these issues, and solar pumping systems will solve these problems.

A solar pumping system is a system that pumps water with electricity generated by photovoltaic modules. The operation of this system is simple in operation with its low cost of maintenance and it's friendly to the environmental impact. Solar pumping systems are useful where there is no grid electricity [1].

The solar photovoltaic arrays are connected directly to the controller which tracks the solar beams falling on the arrays in order to optimize the solar irradiances harnessed by the solar photovoltaic arrays, and converts the DC energy extracted by solar PV to AC energy, and the AC motor shaft is connected to the pump [2].

[1] Department of Mechanical Engineering, Nigerian Army University, Biu, Nigeria
[2] Department of Mechanical Engineering, Ahmadu Bello University, Zaria, Nigeria
[3] National Space Research and Development Agency, Nigeria
[4] Department of Mechatronic Engineering, Bayero University, Kano, Nigeria
[5] Department of Mechanical Engineering, Federal Airports Authority of Nigeria, Abuja, Nigeria
[6] Department of Mechanical Engineering, School of Technology, Binyaminu Usman Polytechnic, Hadejia, Nigeria

Corresponding Author and e–mail address: Jamilu Ya'u Muhammad jamilu.muhammad@naub.edu.ng

The quantity of water pumped by a solar pumping system depends on the total amount of solar irradiances harnessed in a specific time. The flow rate of the water pumped is determined by both the amount of solar energy available and the size of the PV array used to convert that solar energy into electricity [3].

Many works have been done relevant to the solar pumping system among which there are some conducted with hybrid solar PV systems and some others carried out using tracking control systems. According to Ahmad *et al.* [4], the larger pumping systems with a capacity of 150,000 litres/day of water were achieved from an overall head of 10 meters. Manfrida and Secchi [5] designed a solar hybrid system for pumping water and generating electricity. The analysis was performed on two different types of motors: one with variable speed and another with constant speed. It was concluded that at a constant speed of pump with 7000 m^3 of storage capacity and at 42.8% of the energy generated by the PV capacity of 600 KWp can be stored. Whereas the analysis with the variable speed of the pump with 9000 m^3 of storage capacity, at 48.6% of the energy generated by the PV capacity of 600 KWp can be stored. Munir *et al.* [6] designed and constructed a water pump system in a remote area of the Iraqi-Syrian border location for drinking purposes with a capacity of 130 m^3. Alajlan and Smiai [7] designed and constructed two main PV systems, one for the pumping of water and another for the desalination of water by reverse osmosis method and the desalination produces 600 litres/hour.

Solar pumps for irrigation are under-utilized for most of the year because the irrigation farming system is a seasonal farming system, but this system can also be utilized for domestic uses and the rearing of livestock animals.

2. System Description

The study was conducted in Garko Local Government, Kano State. Garko is located in the East of Kano City with coordinates of 11°39'N, 8°54'E and a total population of 162,500 during the 2006 census [8]. The local government occupies a total of 450 square kilometers.

This system consists of solar arrays where the solar irradiance is harnessed as direct current (DC), and these arrays are connected with Maximum Power Point Tracking (MPPT) control which is used to make the solar arrays at an optimum solar trajectory to harness maximum solar irradiances. Solar inverter is used to convert direct current harnessed by solar arrays into alternating current (AC) and it is linked with the MPPT control and finally to the electric motor which is used to run the water pump. Then the water pump actions take water from the well, dam, river or any water source to the overhead tank as shown in Figure 1 below.

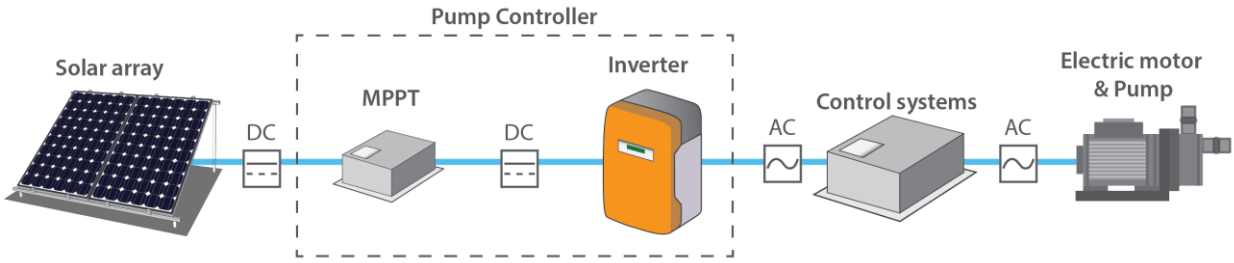

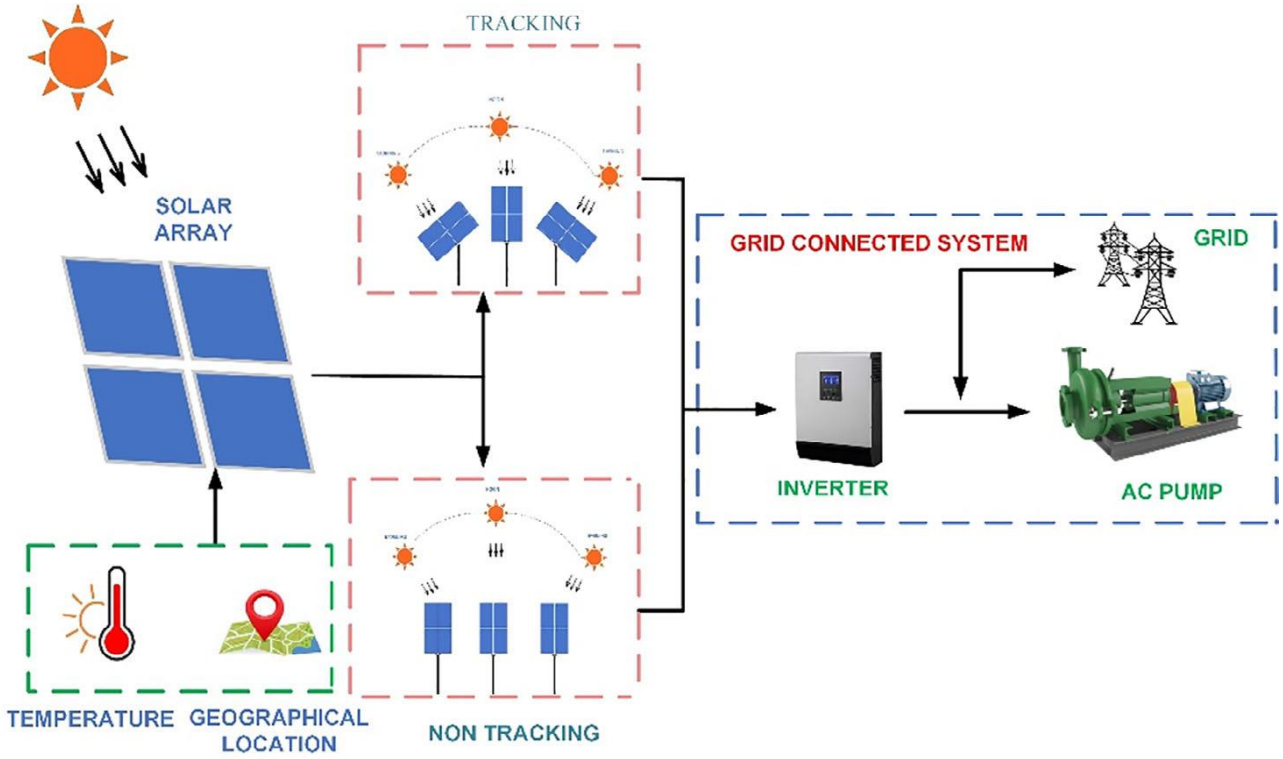

Figure 1: Solar Pumping System Configuration [11]

This system typically uses a surface pump system whereby a shallow well (Tube Well) is used as a source of water. The solar water pump is located above the water level and a suction pipe is used for drawing the water from the water source.

3. Design of the System's Components

To design any pumping system, the quantity of water required per day of the location for the summer and winter seasons must be obtained from the literature.

3.1. Design and Selection of the Water Pump

To select a water pump, the static head, drawdown head, pressure head and losses head were added together to give the total dynamic head as given in equation (1):

$$H_{td} = H_{st} + H_d + H_l + H_p \quad (1)$$

Where:
H_{td} is the total dynamic head (m); H_{st} is the static head (m); H_d is the drawdown head (m); H_p is the pressure head (m) and H_l is the losses head which is the sum of frictional loss head and fitting loss head as in equation (2):

$$H_l = H_f + H_{pf} \quad (2)$$

Where:
H_f is the frictional loss and this can be calculated using the Darcy formula as expressed in the equation (3) as given by [9]:

$$H_f = \frac{32lQ^2K_f}{\pi^2 D^4 g} \quad (3)$$

And H_{pf} is the fitting loss head and it can also be found using the expression given in equation (4):

$$H_{pf} = \frac{8Q^2K_{fi}}{\pi^2D^4g} \quad (4)$$

Where:
l is the length of the pipe (m); Q is the flow rate (m^2/s); K_f is the empirical factor which depends on Reynolds number; D is the diameter of the pipe (m); g is the acceleration due to gravity (m/s^2); and K_{fi} is the fitting loss factor.

The quantity of water the system can pump could be obtained using the expression given in equation (5):

$$Quantity\ of\ water\ pumped\ V = \frac{P_{pv}I_p\eta_{mp}F}{\rho g H_{td}} \quad (5)$$

Where:
P_{pv} is the power of the solar PV array (W); I_p is the average daily solar irradiance ($kWh/m^2/day$); η_{mp} is the efficiency of the motor-pump system; and F is the mismatch array factor.

The hydraulic power exerted on the water pump could be found using the formula given in equation (6) as:

$$Hydraulic\ Power\ P_h = \frac{\rho g H_{td} Q}{3600} \quad (6)$$

3.2. Design of Control System

When the solar PV array harnesses the solar irradiant, the solar irradiance is in DC form and the controller is used to convert the DC form of solar irradiance into AC form. This solar irradiance can be optimized to extract the peak DC load using the Maximum Power Point Technique (MPPT). The voltage across the AC circuit of the load can be calculated using equation (7) as:

$$V_{AC} = \frac{V_{DC}M_a}{\sqrt{2}} \quad (7)$$

Where:
V_{DC} is the DC voltage of the controller (V)

The power output exerted on the AC circuit of the controller can be found using the equation (8):

$$AC\ Power\ Output\ P_{AC} = I_{AC}V_{AC}\sqrt{3} \quad (8)$$

The efficiency of the controller is the ratio of the power output of the AC circuit to the power given out by the DC circuit as given in equation (9):

$$\eta_c = \frac{P_{AC}}{P_{DC}} \quad (9)$$

3.3. Design of the Electric Motor

The electric motor is used to run the water pump due to its less maintenance cost and it's being cheap in the market [2]. The torque used to rotate the shaft of the pump could be obtained using the equation (10):

$$T = K_L W^2 \quad (10)$$

The power liberated to the shaft of the motor is given in equation (11) as:

$$P_m = TW \quad (11)$$

The efficiency of the motor can be found by dividing the power liberated to the motor shaft with the AC circuit power output as given in equation (12):

$$\eta_m = \frac{P_m}{P_{AC}} \tag{12}$$

3.4. Design and Selection of Solar Photovoltaic Arrays

For the solar PV array to pump water from the tube well, the solar modules must be connected in series and parallel.

The number of Solar PV modules connected in series is given in equation (13):

$$No\ of\ PV\ in\ Series\ Connection\ N_{PV-series} = \frac{Pump's\ Motor\ Voltage\ V_{pm}}{Operational\ Voltage\ of\ PV\ Module\ V_{op-PV}} \tag{13}$$

And equation (14) is given to find the number of PV modules connected in parallel as:

$$No\ of\ PV\ in\ Parallel\ Connection\ N_{PV-parallel} = \frac{Pump's\ Peak\ PV\ Voltage}{V_{op-PV} \times N_{PV-series} \times I_{PV} \times F_{De-rating}} \tag{14}$$

The total power output for the solar PV array can be found using the expression given in equation (15) as:

$$PV\ Power\ P_{PV} = \frac{P_h}{I_p \eta_{mp} F} \tag{15}$$

The efficiency of the solar PV array is given in expression (16) as:

$$\eta_{PV} = \frac{P_{PV}}{A_C I_T} \times 100\% \tag{16}$$

The efficiency of the overall system is the product of the efficiency of the solar PV array and the efficiency of the motor pump as expressed in the equation (17) as:

$$\eta_{total} = \eta_{PV} \times \eta_{mp} \tag{17}$$

4. Performance Assessment of the System

The amount of solar irradiance harnessed by the solar PV, the flow rate of the water pumped by the system per hour and the efficiency of the system are parameters measured to ensure that the solar pumping system is working efficiently. In this study, the above parameters were measured for tracking PV and fixed PV of the system for 30 days on both cloudy and sunny days. The average of each measured parameter was used to plot the charts.

Figure 2 presents the performance of the solar pumping system with tracking PV during a sunny day. The test started when the sun started to rise and ended when the sunset at an interval of 30mins for each day. The average amount of solar irradiance, flow rate and efficiency of the system was at maximum values of 1125 W/m^2, 95 m^3/hr and 81 % respectively within the time frame of 12:30 to 13:00 of the day. At 9:30 and 15:30 there was a rapid increase and decrease in the amount of solar irradiance respectively, and this is due to cloud cover during these hours. This result agreed with the research done by Singh and Kumar [12].

Figure 3 shows the performance of the solar pumping system with fixed PV on a sunny day. The test started when the sun started to rise and ended when the sunset at an interval of 30mins for each day. The average amount of solar irradiance, flow rate and efficiency of the system was at maximum values of 867 W/m^2, 54 m^3/hr and 77 % respectively within the time frame of 12:00 to 13:00 of the day. This concurred with the result obtained by Narayana *et al.,* [13].

Figure 4 presents the performance of the solar pumping system with tracking PV during a cloudy day. The test started when the sun started to rise and ended when the sunset at an interval of 30mins for each day. The average amount of solar irradiance, flow rate and efficiency of the system was at maximum values of 836 W/m^2, 52 m^3/hr and 79 % respectively within the time frame of 12:30 to 13:00 of the day. Bouselham et al., [14] obtained similar results to this one.

Figure 5 presents the performance of the solar pumping system with fixed PV during a cloudy day. The test started when the sun started to rise and ended when the sunset at an interval of 30mins for each day. The average amount of solar irradiance, flow rate and efficiency of the system was at maximum values of 826 W/m^2, 50 m^3/hr and 76 % respectively within the time frame of 12:30 to 13:00 of the day. The result obtained is similar to the one obtained by Katan *et al.,* [15].

Finally, it was observed that as the sun rose the amount of water flow rate for both tracked and fixed solar PV was increasing whereas it was decreasing when the sun got to set. Hence, it was found a high variation of the water flow rate simultaneously with the changes in the amount of solar irradiance harnessed by the solar PV, and this concurred with the result obtained by [10]. The total average amounts of water pumped by the tracked and fixed systems were 1370 m^3/day and 804 m^3/day for sunny days. And for cloudy days they were 750 m^3/day and 714 m^3/day. Helmy and Gad [16], Shabaan et al., [17], Jamil [18] and Pande et al., [19] obtained similar results to the results obtained in the present study.

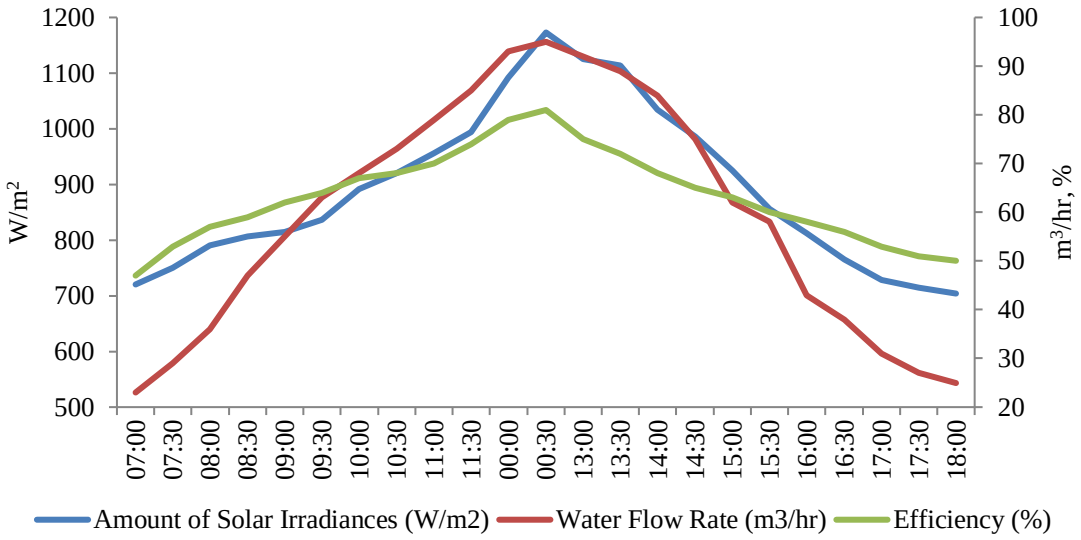

Figure 2: Performance of Tracking Solar Pumping System for Sunny Day

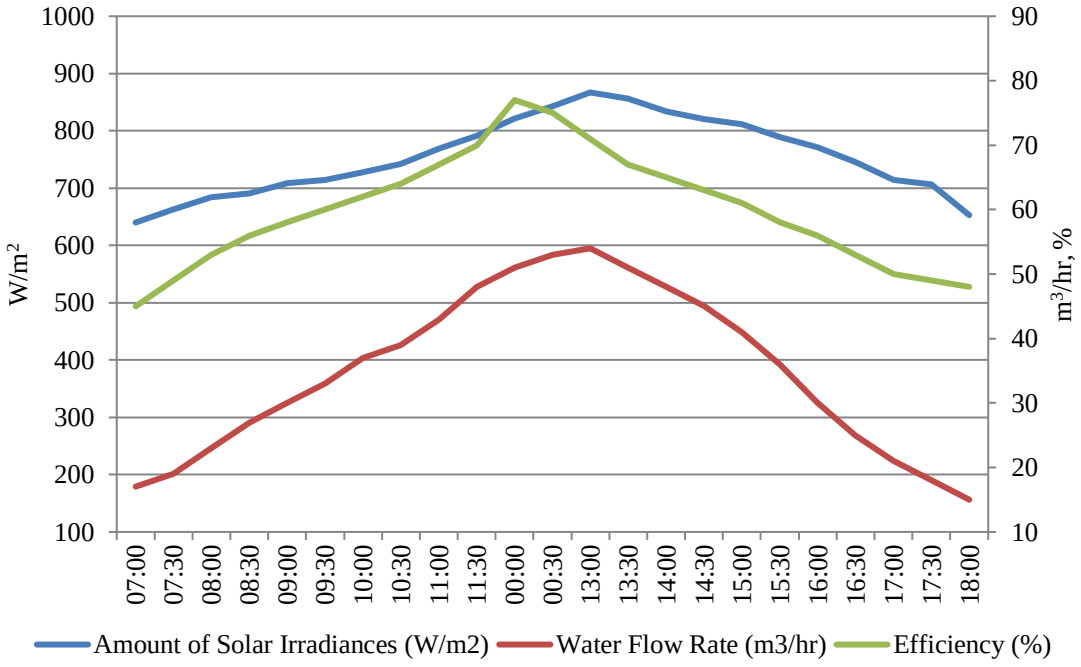

Figure 3: Performance of Fixed Solar Pumping System for Sunny Day

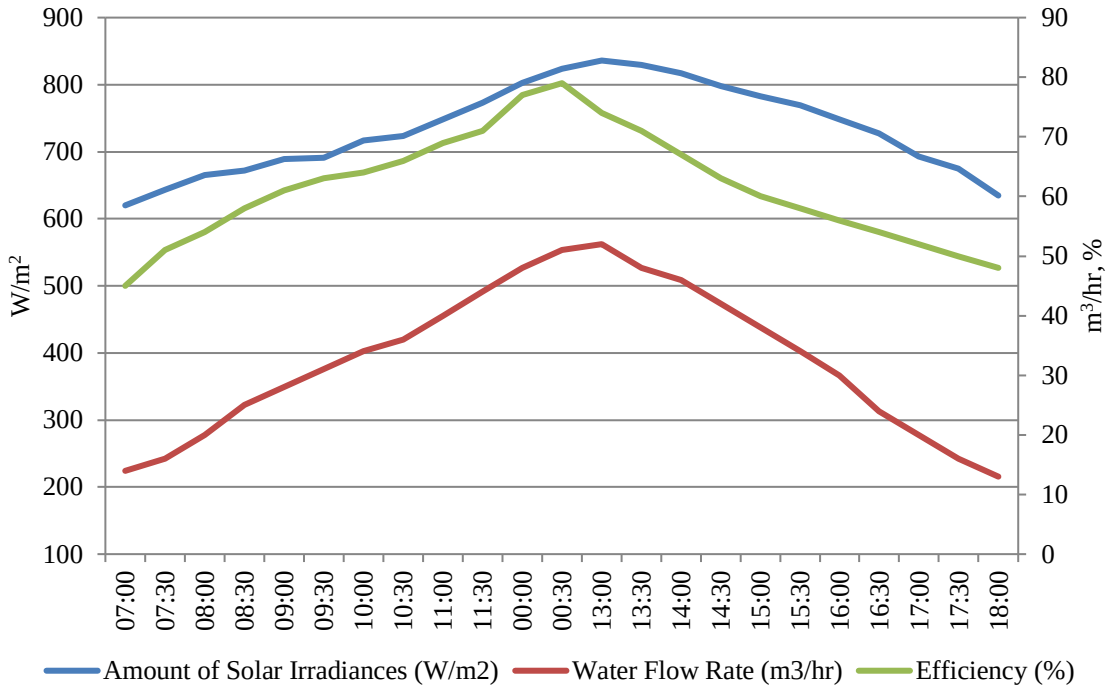

Figure 4: Performance of Tracking Solar Pumping System for Cloudy Day

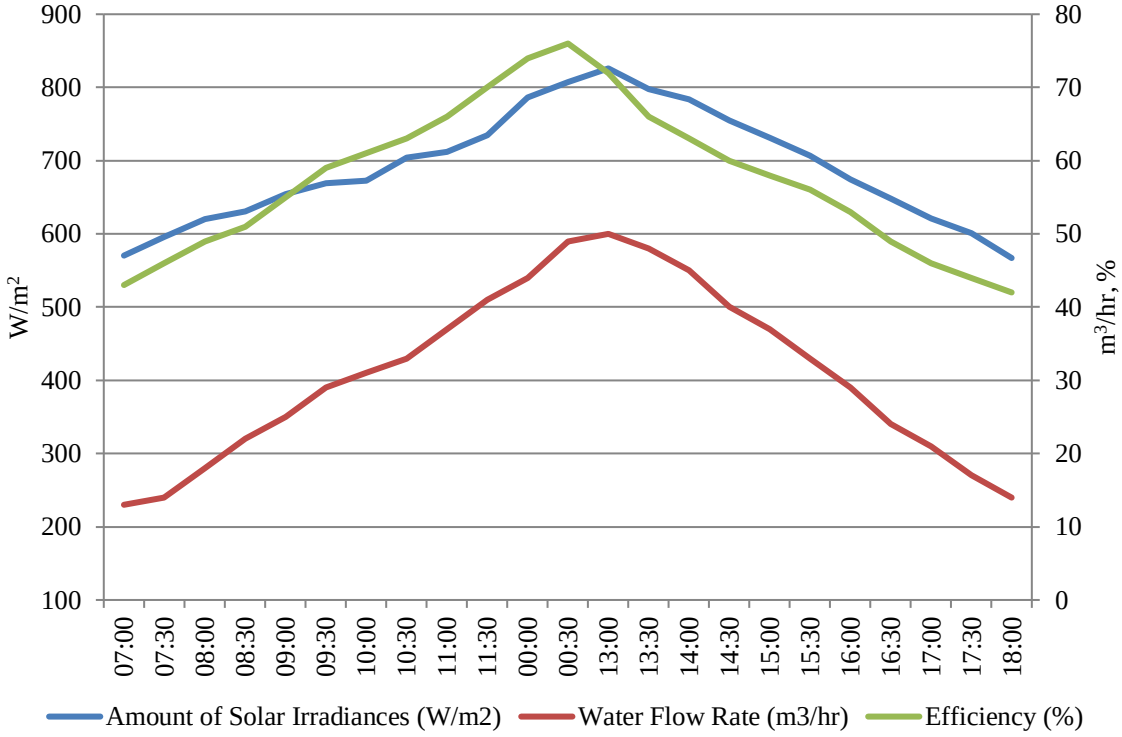

Figure 5: Performance of Fixed Solar Pumping System for Cloudy Day

5. Conclusion and Recommendation

5.1. Conclusion

This study designed the solar pumping system for agricultural use in Kano State Nigeria using maximum power point techniques with a consideration of design factors such as technical, environmental and economic factors. The designed system compared the results obtained by the tracking techniques with the fixed solar PV of the solar pumping system. It was finally observed that the amount of water pumped by the tracking system per day was

much higher than that of fixed solar PV systems, and so were their efficiencies. Although there are some fluctuations in the results of both cloudy days, this is due to the fact that there are cloud covers and heavy rainfall during the time readings are taken from the system and there is little effect of cloud cover on tracking PV solar pump.

5.2. Recommendation

It was recommended in future research to have a higher energy storage battery that can store the solar energy extracted so that the system can overcome the wide gap between the amount of water pump on sunny and cloudy days.

References

[1] Verma, V., & Kumar, A. (2012, December). Power balanced cascaded multilevel inverter fed scalar controlled induction motor pump sourced from photovoltaic source. In *2012 IEEE International Conference on Power Electronics, Drives and Energy Systems (PEDES)* (pp. 1-6). IEEE.

[2] Yousuf, N. B., Salim, K. M., Haider, R., Alam, M. R., & Zia, F. B. (2012, January). Development of a three phase induction motor controller for solar powered water pump. In *2nd International Conference on the Developments in Renewable Energy Technology (ICDRET 2012)* (pp. 1-5). IEEE.

[3] Teresa D. M. (2010). Design of small photovoltaic (PV) solar-powered water pump system. *A Technical Note No. 28 at United States Department of Agriculture (USDA) and Natural Resources Conservation Service (NRCS)*.

[4] Ahmad, Aziz, Zafar K. & Dayanand (2015). Design and Simulation of Photovoltaic water pumping system and MPPT Algorithm in Simulink. *International Journal of Emerging Technology and Advanced Engineering,* 5(4): 539-543.

[5] Manfrida, G. & Secchi, R. (2014). Seawater pumping as an electricity storage solution for photovoltaic energy systems. *Energy,* 69: 470–484.

[6] Munir, A., Al-Karaghouli, A. A. & Al-Douri, A. A. J. (2007). A PV pumping station for drinking water in a remote residential complex. *Desalination,* 209(1-3): 58–63.

[7] Alajlan, S. A. & Smiai, M. S. (1996). Performance and development of PV-plant for water pumping and desalination for remote area in Saudi Arabia. *Renewable Energy*, 8(1-4): 441–446.

[8] NIPOST (2009). Post offices-with map of states and local government areas of Nigeria.

[9] Douglas, J. F., Gasiorek, J. M. & Swaffiel, J. A. (1989). Fluid mechanics. Longman, Harlow: Longman Scientific and Technical, England.

[10] Jamilu, Y. M., Siraj, A., Ibrahim B. K., Mohammed A. G. & Abudharr B. W. (2020). Assessing Performance of Manually Controlled Solar Tracking System in Climate Condition of Kano, Nigeria. *Journal of Investigations on Engineering and Technology,* 3(2): 37-47.

[11] Krishnappa, M. & Natarajan, R. (2021). A review of various components of solar water-pumping system: Configuration, characteristics, and performance. *Int. Trans. Electr. Energ. Syst.,* 31: e13002. https://doi.org/10.1002/2050-7038.13002

[12] Singh, B. & Kumar, R. (2016). Solar photovoltaic array fed water pump driven by brushless DC motor using landsman converter. *IET Renew Power Gener.;* 10: 474-484.

[13] Narayana, V., Mishra, A.K. & Singh, B. (2017). Development of low-cost PV array-fed SRM drive-based water pumping system utilizing CSC converter. *IET Power Electron*; 10: 156-168.

[14] Bouselham, L., Hajji, M., Hajji, B. & Bouali, H. (2016). A MPPT-based ANN controller applied to PV pumping system. *Paper presented at: 2016 International Renewable and Sustainable Energy Conference (IRSEC),* IEEE. pp. 86–92.

[15] Katan, R.E., Agelidis, V.G. & Nayar, C.V. (2018). Performance analysis of a solar water pumping system. *Paper presented at: Proceedings of International Conference on Power Electronics, Drives and Energy Systems for Industrial Growth, volume 1,* IEEE. pp. 81–87.

[16] Gad, H.E. & El-Gayar S. (2018). Performance prediction of a proposed photovoltaic water pumping system at south Sinai, Egypt climate conditions. *Paper presented at: Thirteenth International Water Technology Conference, IWTC13, Citeseer.*

[17] Shabaan, S., El-Sebah, M.I.A. & Bekhit, P. (2018). Maximum power point tracking for photovoltaic solar pump based on ANFIS tuning system. *J. Electr. Syst. Inform. Technol.*; 5:11-22.

[18] Jamil, M. (2012). SPV based water pumping system for an academic institution. *American Journal of Electrical Power and Energy Systems;* 1 (1). http://doi.org/10.11648/j.epes.20120101.11.

[19] Pande, P., Singh, A., Ansari, S., Vyas, S. & Dave, B. (2003). Design development and testing of a solar PV pump-based drip system for orchards. *Renew Energy*; 28: 385-396.